博士論文

Studies on Sodium Borohydride as an Ammonia Absorbing Material

（アンモニア吸蔵材料としての水素化ホウ素ナトリウムに関する研究）

中 嶋　啓 太

広島大学大学院先端物質科学研究科

2019 年 3 月

目次

Ichikawa
International Journal of Hydrogen Energy, **42**, 6173-6180 (2017).

主論文

Abstract

Ammonia (NH_3) is used as various valuable materials such as fertilizer, and recently expected as energy or hydrogen (H_2) carrier. In this thesis, we focused on the NH_3 absorbing materials and NH_3 based H_2 storage system, and studied the following topics as fundamental research to establish the base technologies for practical utilization of NH_3, (1) Spectroscopic analyses for NH_3 absorbing process of Sodium borohydride ($NaBH_4$), and (2) Catalytic effects of NH_3 absorbing materials on H_2 generation of NH_3-LiH system.

(1) Spectroscopic analyses for NH_3 absorbing process of $NaBH_4$

$NaBH_4$ revealed characteristic features as an NH_3 absorbing material differently from the other materials. In this thesis, NH_3 absorption process of $NaBH_4$ has been investigated and discussed by using operando NMR and FT-IR measurements under NH_3 pressures. It is experimentally clarified that the two phases, solid $NaBH_4$ and liquid $NaBH_4$-$2NH_3$, coexist in the plateau region. Furthermore, the NH_3 absorbed state of $NaBH_4$ ($Na(NH_3)_xBH_4$) is also the liquid state in the higher pressure than the plateau pressure. The local chemical states of B-H and N-H bonds in $NaBH_3$ and NH_3 are changed each other with the variation of the NH_3 concentration. Through the analysis based on solution theory for $Na(NH_3)_xBH_4$, it is suggested that the liquid solution is changed from the regular solution to the ideal solution with the increase in the molar ratio of NH_3.

(2) Catalytic effects of NH_3 absorbing materials on H_2 generation of NH_3-LiH system

The additive effects of NH_3 absorbing materials, which are lithium chloride (LiCl), lithium borohydride ($LiBH_4$), and $NaBH_4$, are investigated

to improve the kinetic properties of the H_2 storage system composed of NH_3 and lithium hydride (LiH). The NH_3 absorbing materials reveal a significant catalytic effect on the H_2 generation reaction. Particularly, $NaBH_4$ is the most effective, and then the reaction yield reaches to more than 90% for 12 h, although the yield in the case of LiH without catalysts is less than 50% for 12 h. Furthermore, the catalysis is strongly related to the NH_3 absorption properties of the catalysts. As the catalytic mechanism, it can be proposed that the NH_3 condensation state is realized in the catalysts and improves the kinetic properties.

Contents

1 Introduction

1.1 Ammonia

Hydrogen for sustainable energy society

Fossil fuels, such as coal, petroleum, and natural gas, has been utilized for our lives since the late 1800s. In Japan, about 90% of energy consumption is covered by fossil fuels.[1] This value is almost the same as the ratio of energy consumption in the world. However, the fossil fuels are finite in the earth and will be depleted by continuing the current energy system. Furthermore, carbon dioxide, which is greenhouse gas, is generated by the combustion of fossil fuels. Therefore, it is necessary to change a consumer society based on fossil fuel to a sustainable energy society based on renewable energy such as solar and wind energy.

Renewable energy is fluctuated with time and localized at special area, for instance, solar energy cannot be used at night or in bad weather. In other words, it is difficult to use renewable energy with our demand. Thus, for stable supply of renewable energy, effective secondary energy such as hydrogen and battery is required.[2] Particularly, we focused on hydrogen because of the following reasons.

- Hydrogen has higher gravimetric energy density than battery, furthermore, the value is comparable to liquid fuel like gasoline.
- Hydrogen can be generated from renewable energy by using various methods such as water electrolysis, thermochemical water splitting, and photocatalytic water decomposition.

- Hydrogen can be used as energy by combustion or fuel cell, and then, only water is generated. Thus, it can be regarded as clean energy media.

From above reasons, hydrogen is recognized as promising energy medium to establish sustainable energy society. However, it is necessary to develop the basic technologies such as hydrogen production, storage/transportation, and utilization. In particular, since the volumetric energy density of hydrogen is very low due to gaseous state in ambient conditions. Therefore, research and development of hydrogen storage techniques are an important issue. So far, compressed hydrogen, liquid hydrogen, and hydrogen storage materials, are studied as compact storage techniques.[3] Hydrogen storage materials such as metal hydrides,[4-6] complex hydrides[7-9] and carbon materials[10-12], can store hydrogen with higher volumetric hydrogen density than other techniques.

Ammonia as a hydrogen carrier

Recently, ammonia (NH_3) is expected as a hydrogen storage material (hydrogen carrier) to transport large amount of hydrogen because of following reasons.[13-17]

- Ammonia has high gravimetric and volumetric hydrogen density, compared with other hydrogen storage materials, as shown in Figure 1.1. The gravimetric hydrogen density is 17.8 wt.%, and the liquid phase of ammonia is 1.5 times higher volumetric hydrogen density than that of liquefied hydrogen.[13]

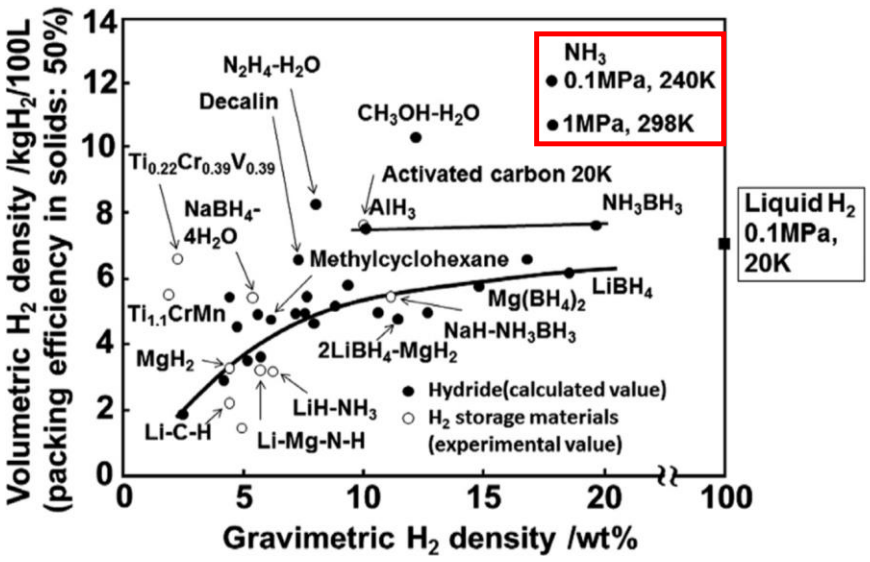

Figure 1.1 Hydrogen densities in various hydrogen carriers

- Ammonia is easily liquefied by compression. Figure 1.2 shows the vapor pressure of ammonia at the different temperatures. Liquefied pressure at 20 °C is 0.86 MPa although hydrogen requires below -240 °C, which is critical point.[13, 18]

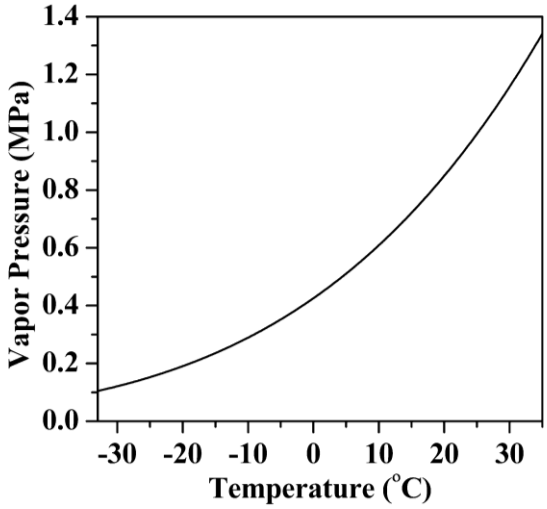

Figure 1.2 The vapor pressure of NH_3 at various temperatures

- It is a carbon-free material because ammonia does not emit greenhouse gas like carbon dioxide ideally during combustion, as follows,[15]

  $4NH_3 + 3O_2 \rightarrow 2N_2 + 6H_2O.$ (1.1)

- A massive synthesis method has been established and it is industrialized about 100 years ago.[19] The annual production amount of ammonia is 1 and 170 million tons in Japan and world, respectively.
- Transportation and storage infrastructure has been established because ammonia is used as a material of fertilizers for a long time.

On the other hand, the technical research and development to practically utilize ammonia as the hydrogen carrier is required. For instance, in Japan, four themes related to ammonia as an energy (hydrogen) carrier proceed in a cross-ministerial Strategic Innovation Promotion Program (SIP) since 2014.[20] The themes are (i) development of ammonia synthesis process from CO_2 free Hydrogen, (ii) basic technology for hydrogen station utilizing ammonia, (iii) ammonia fuel cell, (iv) ammonia direct combustion.[20]

Ammonia production

Ammonia and the products synthesized from ammonia have played a lot of important roles as various ways such as fertilizers, explosives, fibers, resins, animal feed, and nitrogen oxide scavenger. More than 80% is particularly used as a fertilizer. Thus, ammonia is indispensable to our lives. Ammonia is synthesized from nitrogen and hydrogen. Nitrogen can be obtained from air. Hydrogen is produced from hydrocarbon (C_mH_n) as a raw material in two processes of steam-reforming reaction and gas shift reaction. In the steam-reforming reaction, H_2 and carbon monoxide (CO) are generated from C_mH_n,

such as methane (CH_4), and water (H_2O) as following equation,

$$C_nH_m + nH_2O \leftrightarrows nCO + (m/2 + n)H_2 \quad (1.2)$$

The reaction is industrially operated at a high temperature around 800 °C by the use of nickel based catalysts.[21, 22] Furthermore, CO and H_2O are converted to CO_2 and H_2 by the following water-gas shift reaction,

$$CO + H_2O \leftrightarrows CO_2 + H_2 \quad (1.3)$$

This reaction is the exothermic reaction for hydrogen production. The reaction proceeds around 300 °C by iron or cupper based catalysts.[23, 24] Ammonia production was industrialized by BASF in 1913, and the production method is called Haber-Bosch process as following equation,[25]

$$N_2 + 3H_2 \leftrightarrows 2NH_3. \quad (1.4)$$

The air is used as a raw material of N_2. O_2 in the air reacts with CH_4, which is the remain of a raw material of H_2, and is treated as CO_2 or H_2O. This reaction (1.4) requires a solid catalyst, such as magnetite (Fe_3O_4) and is operated at high temperatures (400-500 °C) and pressures (5-20 MPa).[25, 26] In this achievement, Haber and Bosch were awarded the Nobel Prize in 1918 and 1931, respectively. Although ammonia (hydrogen) is currently produced by fossil fuels as mentioned above so far, pilot plants of green ammonia, which is synthesized from hydrogen produced by the renewable energy, recently began to operate in the UK and Japan,[27] and new demonstration plants will be worked in Australia, Morocco, Denmark, and Netherland.[28-32]

Ammonia decomposition

The techniques of the ammonia decomposition to generate hydrogen as fuels, such as thermolysis, electrolysis, and ammonolysis, have been studied.

Ammonia can be decomposed by thermolysis and the reaction is expressed by equation (1.4). The conversion rate of ammonia is determined by thermodynamic equilibrium.[33, 34] In Table 1.1, the relationship between the reaction temperature and the equilibrium ammonia conversion at normal pressure (1.01325×10^5 Pa) is shown, and the conversion rate reaches to more than 99 % around 400 °C. Various catalysts such as Pt,[34, 35] Ru,[34, 36-39] Fe,[34, 40] and Ni,[34, 41, 42] have been studied to improve the kinetics.

Table 1.1 The equilibrium ammonia conversion at the various temperatures

Temperature (°C)	Conversion (%)
250	89.21
300	95.69
350	98.12
400	99.11
450	99.53
500	99.74

Liquid ammonia is theoretically decomposed by electrolysis at 0.077 V. This voltage is much smaller than that of water (1.23 V), indicating that the electrolysis of ammonia requires 94% lower energy than the water electrolysis.[43-46] The decomposition reactions on negative and positive electrode are described as the following equations in the case of alkaline metal amides as electrolytes,[43]

Negative: $3NH_3 + 3e^- \rightarrow 3/2H_2 + 3NH_2^-$, (1.5)

Positive: $3NH_2^- \rightarrow 1/2N_2 + 2NH_3 + 3e^-$. (1.6)

As overall reaction, liquid ammonia could be electrochemically decomposed

with the generation of hydrogen and nitrogen.

In addition to the above techniques, ammonia can be decomposed by ammonolysis reaction. Ammonia reacted with alkaline metal hydride to generate H_2 and alkaline metal amide. The further detail is described in section 1.4.

1.2 Ammonia absorbing materials

Various kinds of metal halides MX_m or borohydrides $M(BH_4)_m$ react with NH_3 to form ammine complex as follows,

$$MX_m + n\mathrm{NH_3} \leftrightarrows M(\mathrm{NH_3})_n X_m, \quad (1.7)$$

$$M(\mathrm{BH_4})_m + n\mathrm{NH_3} \leftrightarrows M(\mathrm{NH_3})_n(\mathrm{BH_4})_m. \quad (1.8)$$

These materials are studied for a long time. Biltz et al. and Ephraim et al. reported on ammonia absorbing phenomena of metal halides about 100 years ago.[47-49] The ammonia absorbing materials have been investigated in various fields such as hydrogen storage, ammonia removal, chemical heat pump, and ammonia storage so far.

Hydrogen storage

The hydrogen storage properties of the ammine complex of various borohydrides, such as $Li(NH_3)BH_4$[50, 51], $Mg(NH_3)_nBH_4$ (n=1, 2, 3, 4, 5, 6)[52, 53], $Ca(NH_3)_2(BH_4)_2$[54], $Al(NH_3)_n(BH_4)_3$ (n=4, 6)[55, 56], $Mn(BH_4)_2{\cdot}nNH_3$ (n=1, 2, 3)[57], $Ti(NH_3)_n(BH_4)_3$ (n=3, 5)[58], $V(NH_3)_3(BH_4)_3$[59], $Y(NH_3)_4(BH_4)_3$[60], $Zr(NH_3)_8(BH_4)_4$[61], $Li_2Al(NH_3)_6(BH_4)_5$[56], $Li_2Mn(NH_3)_6(BH_4)_4$[57], $Mg_{1-x}Mn_x(NH_3)_6(BH_4)_2$[57], $Li_2Ti(NH_3)_5(BH_4)_5$[58], $LiSc(NH_3)_4(BH_4)_4$[59], and $Li_2Mg(NH_3)_6(BH_4)_4$[62], have been investigated. $Li(NH_3)BH_4$ is the representative ammine complex for hydrogen storage. About 50 years ago, Sullivan et al. investigated the NH_3 pressure-composition isotherms (PCI) for $LiBH_4$, as the result, $LiBH_4$ absorb NH_3 and form ammine complex with various compositions, $Li(NH_3)_nBH_4$ (n = 1, 2, 3, 4).[63] The structural analysis was carried out for $Li(NH_3)BH_4$ by Johnson et al., and the absorption of NH_3 in $LiBH_4$ leads a tetrahedral coordination of three BH_4^- units and one NH_3 molecule around the

central Li atom. Here, the distance between H in NH_3 molecule and H in BH_4^- is approximately 2.3–2.5 Å, suggesting that there are some interaction, such as dihydrogen bonding, between $H^{\delta+}$ in NH_3 and $H^{\delta-}$ in $LiBH_4$.[64, 65] Actually, such interaction is also observed by structural studies in other ammine complexes of borohydride like $Ca(NH_3)_2(BH_4)_2$ and $Li_2Al(NH_3)_6(BH_4)_5$.[54, 56] Furthermore, Chen et al. suggested that this combination between NH and BH in $Li(NH_3)_{4/3}BH_4$ leads to the hydrogen generation reaction, not ammonia generation reaction as following equations,[51]

$$Li(NH_3)_{4/3}BH_4 \rightarrow 2/3BNH_x + 1/9LiBH_4 + 2/9Li_4BN_3H_{10} + (8\text{-}x)/3H_2 \quad (1.9)$$

$$\rightarrow 2/3BN + 1/3Li_3BN_2 + 4H_2 \quad (1.10)$$

Here, $Li(NH_3)_{4/3}BH_4$ is not formed based on the above PCI measurement by Sullivan et al., however, the composition was found by the experiments in a closed system under NH_3 atmosphere. In this case, 17.8 wt% of H_2 can be released from the $Li(NH_3)_{4/3}BH_4$ in the temperature range of 135 to 250 °C with the assistance of Co catalyst.

NH_3 removal

When NH_3 is used as a H_2 carrier, NH_3 should be decomposed into mixed gas of N_2 and H_2 with a small amount of residual NH_3 at utilization sites.[66-68] Current polymer electrolyte membrane (PEM) fuel cells are seriously poisoned even by a small amount of NH_3.[69] According to ISO14687-2, less than 0.1 ppm of NH_3 concentration can be accepted for PEM fuel cell vehicles (FCVs) as shown in Table 1.2.[66, 70] Here, ISO is International Organization for Standardization and an agency that establishes international standards. Thus, it

is necessary to remove NH_3 from the fuel gases obtained by the NH_3 cracking to produce high purity H_2. In SIP for the technical research and development to practically utilize NH_3 as the energy carrier in Japan, the materials for the NH_3 removal are investigated as the basic technology for hydrogen station utilizing NH_3. Based on the above background, ammonia absorbing materials are one of promising NH_3 removal media. In addition, these materials with low plateau pressure for the reaction with NH_3 are utilized as NH_3 trapping materials for emergency situations such as leakage of large amount of NH_3 form the infrastructure as well.

Table 1.2 Specification of hydrogen fuel for FCV （ISO 14687-2）

Species	Concentration (ppm)
Total hydrocarbon	2
Water	5
Oxygen	5
Nitrogen + Argon	100
Helium	300
Carbon dioxide	2
Carbon monoxide	0.2
Total sulphur compound	0.004
Formaldehyde	0.01
Formic acid	0.2
Ammonia	0.1
Total halogenated compounds	0.05

Heat storage

The ammonia absorbing materials have been studied to be utilized for chemical heat storage. Here, the ammonia absorption and desorption reactions generally proceed with the exothermic and endothermic, respectively. Chemical heat pump is operated in two processes of heat output and heat storage as shown in Figure 1.3. In the heat output process, the heat required at evaporator is supplied to vaporize ammonia, which reacts with the ammonia absorbing materials and releases heat at the reactor. Thus, ammonia absorption reaction is utilized for the heat output. In the heat storage process, heat is supplied to the reactor with regenerating ammonia, and the ammonia is stored in the condenser. Thus, ammonia desorption reaction is utilized for the heat storage. When ammonia absorbing materials and ammonia are separated, the heat could be stored for a long time because the reaction does not proceed.

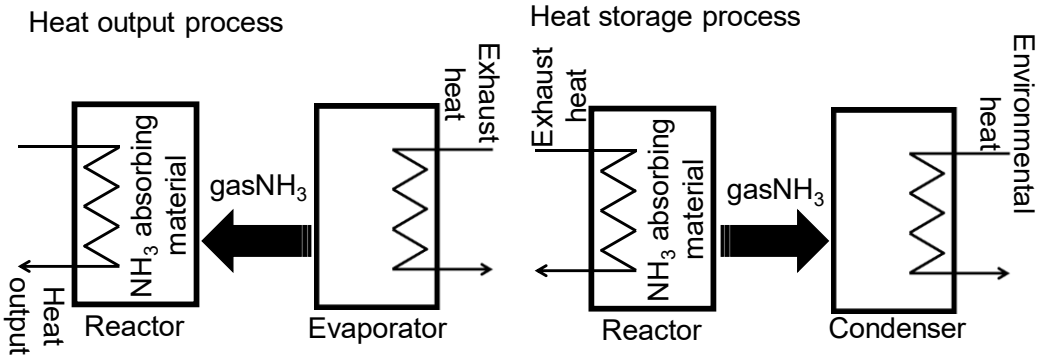

Figure 1.3 The image of heat storage using NH_3 absorbing material

Ammonia storage

Some kinds of materials store NH_3 to form solid ammine complex, and then NH_3 can be desorbed reversibly. Thus, NH_3 is stored in thermodynamically stable solid phase, indicating that the safety and health issues of liquid ammonia with relatively high pressure could be solved as shown in Table 1.3.

Table 1.3 Vapor pressures, IDLH (immediately dangerous to life or health), apparent toxicity (= vapor pressure/IDLH*10^4), state, and NH_3 density of energy carriers at 20 °C

Materials	Vapor pressure (kPa) at 20 °C	IDLH (ppm)	Apparent toxicity	State	NH_3 density (kg/L)
Gasoline	50.6	750	675	Liquid	-
Ethanol	5.86	3300	18	Liquid	-
liq. NH_3	860	300	28667	Liquid	0.61
$Mg(NH_3)_6Cl_2$	0.14	300	5	Solid	0.62

In the case of magnesium chloride ($MgCl_2$) as a typical ammonia absorbing material, the toxicity is drastically reduced compared with liquid NH_3 at room temperature by storing NH_3 in $MgCl_2$ as $Mg(NH_3)_6Cl_2$, and the apparent toxicity of $Mg(NH_3)_6Cl_2$ is less than gasoline.[13] This is because the vapor pressure of $Mg(NH_3)_6Cl_2$ is much lower than that of liquid ammonia. Furthermore, the volumetric ammonia densities of ammine complex such as $Mg(NH_3)_6Cl_2$ and $Ca(NH_3)_8Cl_2$ are comparable with that of liquid ammonia.[71] Thus, by using the above materials, ammonia can be controlled and utilized safely for practical applications. On the other hand, high temperature heat is required for ammonia desorption reaction because the ammine complex phases are

thermodynamically stable. NH_3 in $Mg(NH_3)_6Cl_2$ is desorbed in 3 steps at high temperature range as follows,[72]

$$Mg(NH_3)_6Cl_2 \rightarrow Mg(NH_3)_2Cl_2 + 4NH_3 \quad \text{around 200 °C,} \qquad (1.11)$$

$$\rightarrow Mg(NH_3)\,Cl_2 + NH_3 \quad \text{around 350 °C,} \qquad (1.12)$$

$$\rightarrow MgCl_2 + NH_3 \quad \text{around 400 °C.} \qquad (1.13)$$

In the case of $Ca(NH_3)_8Cl_2$, the NH_3 desorption reaction proceeds in 4 steps at the temperature range of 25-300 °C.[72]

1.3 $NaBH_4$ as an ammonia absorbing material

As described above, many researchers in various research fields focused on ammonia absorbing materials for different purposes. Recently, Aoki et al. have systematically investigated the NH_3 absorption properties of various kinds of halides and borohydrides by using PCI measurements as a fundamental research (Table 1.4).

Table 1.4 Ammonia absorption capacity and equilibrium pressure (P_{eq}) of various materials at 20 °C

Material	NH_3 capacity (mol/mol)	P_{eq} (MPa)
LiF	-	＞0.800
LiCl	4	0.178
LiBr	2	＜0.001
CaF_2	-	＞0.800
$CaCl_2$	8	0.030
NaI	5	0.055
$NiCl_2$	6	＜0.001
$NiBr_2$	6	＜0.001
NaCl	-	＞0.800
KBr	-	＞0.800
MgF_2	-	＞0.800
$LiBH_4$	3	＜0.001
$NaBH_4$	2	0.090
KBH_4	-	＞0.800
$Ca(BH_4)_2$	5	＜0.001
$Mg(BH_4)_2$	5	＜0.001

They found that the correlation between the plateau pressure and the electronegativity of cation or anion in the metal halides or borohydrides. On the other hand, it is difficult to explain the NH_3 absorbing properties like NH_3 capacity (coordination number of NH_3) and equilibrium pressure by the electronegativity for all the NH_3 storage materials. For example, crystal structure, ion size, NH_3 absorbed state (solid or liquid), and chemical state should be considered as control factors for the NH_3 absorption as well. In this work, we focused on sodium borohydride ($NaBH_4$) as an NH_3 absorbing material to understand the relation of the NH_3 absorbed state and chemical state in the NH_3 absorption process. $NaBH_4$ revealed characteristic features differently from the other materials in the PCI experiments. After the plateau region, the vapor pressure was linearly increased with the introduction of NH_3. In this section, the properties of $NaBH_4$ as an ammonia absorbing material discussed in previous research is described below. Based on PCI measurements, 1 mol of $NaBH_4$ absorbs 2 mol of NH_3 at 90 kPa at 20 °C as following equation,[73]

$$NaBH_4 + 2NH_3 \leftrightarrow Na(NH_3)_2BH_4, \quad (1.14)$$

and the plateau pressure was lower than that of liquid ammonia (860 kPa, 20 °C) as shown in Figure 1.4. Possibility that the ammine complex of $NaBH_4$ could be liquid phase is suggested because of the slope-like profile of PCI curve at high NH_3 concentration region. Furthermore, the PCI measurements were carried out at different temperatures, and ΔH^0 and ΔS^0 were obtained from the relationship between the experimental temperature and the equilibrium pressure by the Van't Hoff plot, and the values were evaluated to be −29 kJ/mol and −98 J/(mol K), respectively. Aoki et al. suggested that ΔS^0 was almost the same as

that of liquefaction of NH_3, indicating that a degree of freedom corresponding to the NH_3 molecules in $Na(NH_3)_2BH_4$ is similar to that of liquefied NH_3. Zhang et al. reported the cycle properties in $NaBH_4$-NH_3 system as shown in Figure 1.5.[74] It is suggested that ammonia absorption and desorption processes proceed reversibly and could be controlled by only pressure at 20 °C without thermal activation. Here, $NaBH_4$ is observed from the X-ray diffraction measurements before and after PCI measurement at 20 °C, indicating that the NH_3 absorption and desorption reactions proceed without side reactions. On the other hand, the detailed reaction mechanism of $NaBH_4$ and NH_3 system is not understood yet because the NH_3 absorbed state of $NaBH_4$ is thermodynamically unstable without NH_3 pressure around room temperature. Therefore, the analyses must be performed under NH_3 atmosphere to know details of the NH_3 absorbed state.

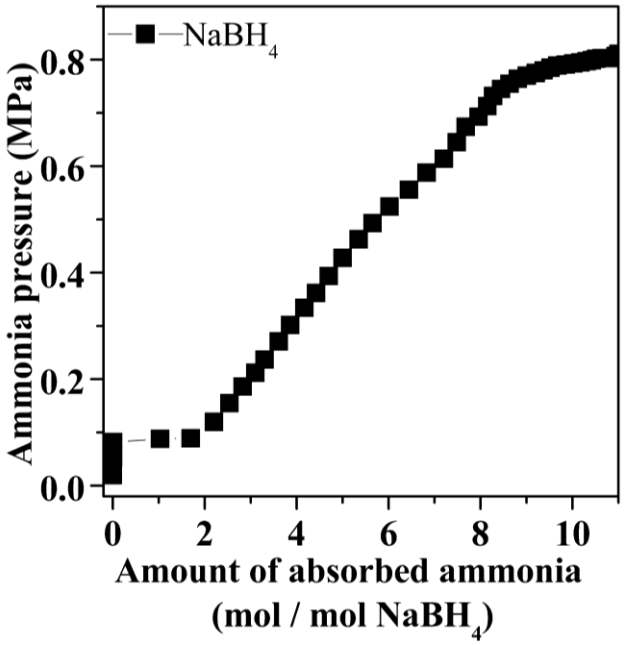

Figure 1.4 The NH_3 absorption property of $NaBH_4$ at 20 °C

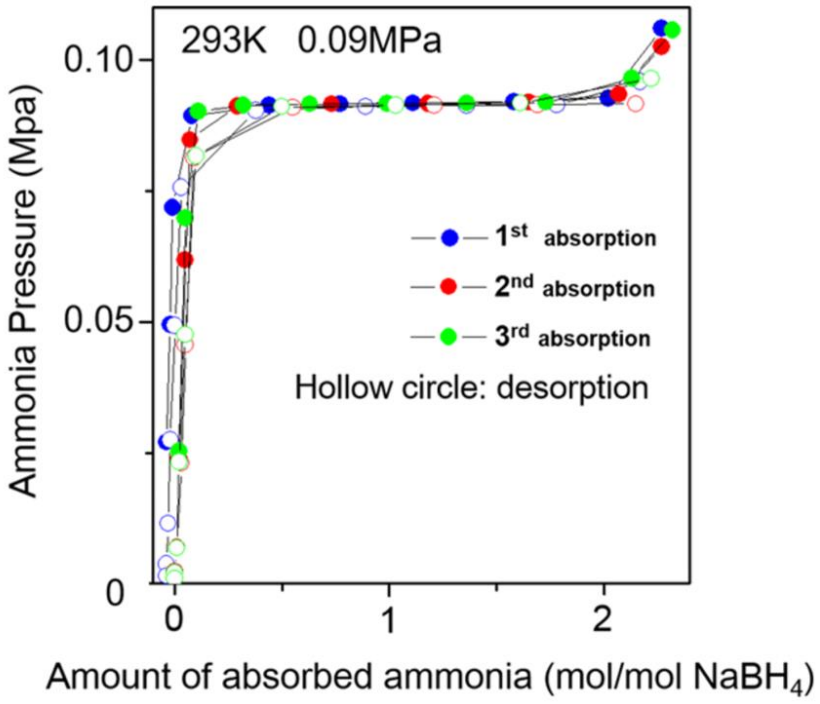

Figure 1.5 The cycle properties of NH_3 absorption and desorption in $NaBH_4$-NH_3 system

1.4 NH_3-LiH system as hydrogen storage system

In 1910, Dafert et al. reported the reaction between lithium nitride (Li_3N) and H_2, and they described the reaction as follows[75],

$$Li_3N + 2H_2 \rightarrow Li_3NH_4. \quad (1.15)$$

Ruff et al. reported later that the reaction product Li_3NH_4 was a mixture of $LiNH_2$ and 2LiH.[76] After about 100 years, Chen et al. have focused on this system as a hydrogen storage system because of its high gravimetric density (10.4 wt%) and investigated the hydrogen desorption and absorption reactions described as follows[77-81],

$$Li_3N + 2H_2 \leftrightarrow LiNH_2 + 2LiH. \quad (1.16)$$

The hydrogen absorption and desorption reactions reversibly proceed below about 450 °C, and this reaction was composed of the following two reactions,

$$Li_3N + H_2 \leftrightarrow Li_2NH + LiH, \quad (1.17)$$

$$Li_2NH + H_2 \leftrightarrow LiNH_2 + LiH. \quad (1.18)$$

In fact, in the thermogravimetry analysis, the weight loss with 2 steps around 170 and 430 °C is observed in the desorption process[77]. Here, the standard enthalpy of formation $\Delta_f H^0$ of Li_3N, Lithium imide (Li_2NH), Lithium amide ($LiNH_2$), Lithium hydride (LiH), and H_2 are -165, -222, -176, -91, and 0 kJ/mol, thus, the enthalpy changes ΔH^0 for reactions (1.16), (1.17), and (1.18) could be calculated to -97, -148 and -45 kJ/mol H_2, respectively[77, 82]. Ichikawa et al. focused on reaction (1.18) and investigated the properties in further detail because the hydrogen capacity is still high, where it is 6.5 wt%, and the reaction could be controlled under moderate conditions due to the small enthalpy changes of reaction. Furthermore, it is proposed that reaction (1.18) proceeds by the two-step reactions mediated by NH_3 as follows[83, 84],

$$2LiNH_2 \leftrightarrow Li_2NH + NH_3, \quad (1.19)$$

$$NH_3 + LiH \leftrightarrow LiNH_2 + H_2. \quad (1.20)$$

$LiNH_2$ is first decomposed to Li_2NH and NH_3, and then the generated NH_3 molecule at the surface of $LiNH_2$ immediately reacts with LiH to form $LiNH_2$ and H_2. In this thesis, we focused on the NH_3-LiH system (reaction (1.20)), and then the further detail of this reaction as a hydrogen storage system are described below.

The NH_3-*M*H system can be expressed by the following equation,

$$NH_3 + MH \leftrightarrow MNH_2 + H_2. \quad (1.21)$$

These systems are systematically investigated as hydrogen storage system [85-88]. Yamamoto et al. investigated the hydrogen generation and regeneration properties of these systems, where *M* is lithium (Li), sodium (Na), and potassium (K).[86] The gravimetric hydrogen density is 8.1, 4.9, and 3.5 wt%, respectively. Furthermore, in the NH_3-LiH system, the volumetric hydrogen density reaches to 4.5 kg/100 L, assuming that NH_3 is the liquid state and the packing density of solid state LiH is 60%. This value is higher than the volumetric density of hydrogen compressed by 70 MPa of pressure, which is 3.9 kg/100 L. Therefore, the NH_3-LiH system is attractive as hydrogen storage technique because of its high gravimetric and volumetric density. The thermodynamic parameters ($\Delta_f H^0$ and S^0) of the materials relating to this reaction are shown in Table 1.5.[18, 89] Accordingly, in *M*H-NH_3 system, the enthalpy change of the dehydrogenation reaction ΔH^0 is calculated to be -39 (Li), -22 (Na), and -25 (K) kJ/ mol H_2, respectively. Therefore, the hydrogen desorption reaction thermodynamically proceeds at room temperature because it is an exothermic reaction. On the other hand, the hydrogen absorption by the

endothermic reaction is achieved below 300 °C under the H_2 flow condition.

Table 1.5 Enthalpy and entropy changes of the materials relating to reaction (1.21)

Material	$\Delta_f H^0$ (kJ/mol)	S^0 (J/mol*K)
LiH	-91	20.03
NaH	-56	40.03
KH	-58	50.18
NH_3(gas)	-46	192.77
$LiNH_2$	-176	-
$NaNH_2$	-124	-
KNH_2	-129	-
H_2(gas)	0	130.68

The hydrogen absorption reaction is exothermic reaction in conventional reversible hydrogen storage systems, indicating that these thermodynamic properties are characteristics in the *M*H-NH_3 systems. Figure 1.6 shows the relationship between reaction yield and reaction time at room temperature for hydrogen desorption reaction.[86]

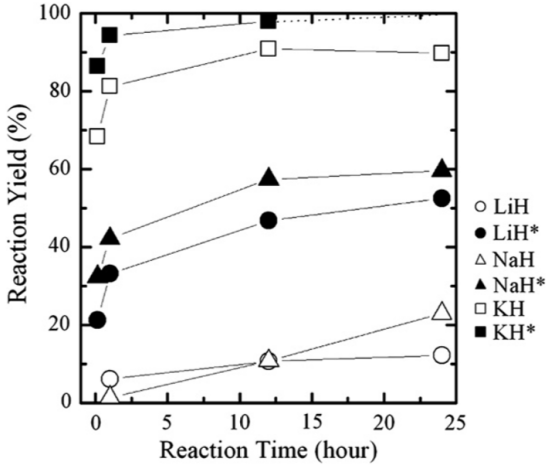

Figure 1.6 The reaction yields of H_2 generation for NH_3-*M*H system (*M*=Li, Na, K) at 1, 12, and 24 h

Here, the open symbols indicate the reaction yields of the reaction between each pristine sample and NH_3. The NH_3-KH system revealed the highest reactivity and the reaction yield achieved about 90% after 12 h at room temperature, on the other hand, the reaction yield is only about 10 or 20% even in 24 h for NH_3-LiH and NH_3-NaH systems. Namely, the reactivity of the NH_3-LiH system with the highest hydrogen capacity is very poor. Therefore, an improvement of kinetic properties is a critical issue for the NH_3-LiH system.

The ball-milling is used as a technique to improve the kinetics on the hydrogen generation of the NH_3−LiH system.[86, 90-92] The closed symbol of LiH in Figure 1.6 is the reaction yield between the ball-milled LiH and NH_3, and the reaction rate was improved, resulting in about 50 % of reaction yield for 24 h. Generally, when the ball-milling is used in the gas-solid reactions, the kinetic properties are controlled by surface reaction and atomic diffusion process. Actually, it is reported that the surface of pristine LiH was covered with LiOH, and a fresh surface of LiH appeared after the ball-milling, where this phenomena are characterized by the X-ray photoelectron spectroscopic analysis.[91] Moreover, the correlation between particle size and hydrogen generation properties on NH_3-LiH system is investigated, and it is clarified that the reaction proceeds faster as the particle size is smaller.[90] On the other hand, even if the ball-milling is performed for NH_3-LiH system, the reaction proceeds only 50%. This is because $LiNH_2$ is formed on the LiH surface as the reaction progresses. Actually, the reaction yield achieved about 100% by the ball-milling under NH_3 atmosphere because of the dynamic destruction of $LiNH_2$ layers on the surface and the simultaneous reduction of the crystalline size.[87, 90]

The addition of catalysts is another effective technique to modify kinetics,

and catalytic effects of various chlorides, potassium compounds, and amides have been investigated.[92-95] Among them, titanium(III) chloride ($TiCl_3$) is the most effective as a catalyst to improve the reaction kinetics, and then the reaction yield reaches to 80% for the 24 h as shown in Figure 1.7.[94]

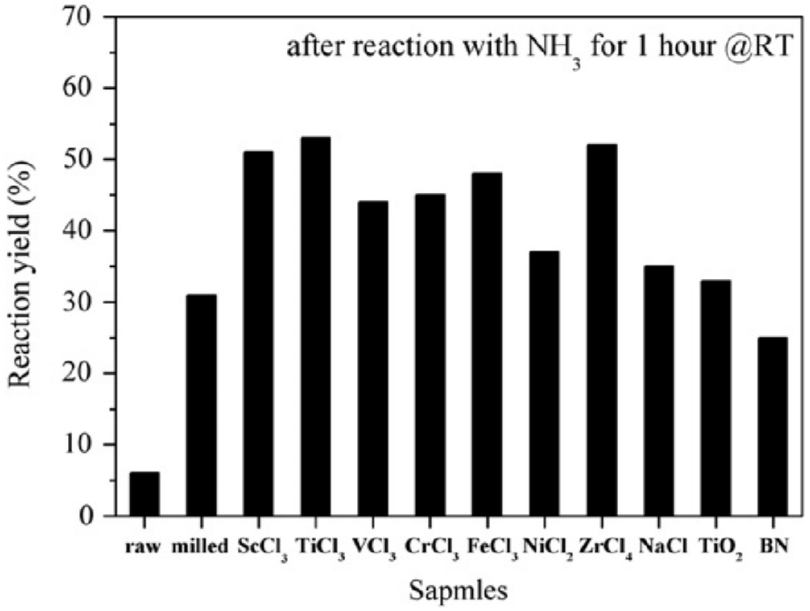

Figure 1.7 Reaction yield of the raw, milled, and various additives dispersing LiH for the reactions with NH_3 for 1 h at room temperature

On the other hand, the lithium chloride (LiCl) formation is clarified after the ball-milling process to disperse $TiCl_3$ into LiH, suggesting that $TiCl_3$ is mechanochemically changed to LiCl and Titanium (Ti) or Ti-compound such as Ti(II) hydride (TiH_2) during the milling. However, it is not yet understood what material possesses the catalytic effect. In common understanding, transition metal catalysts such as Ti possibly improve kinetics on gas−solid reactions, especially a dissociation process of the gaseous molecule is activated. Here, it was reported that LiCl absorbs NH_3 molecules to form the ammine

complex phase like magnesium chloride ($MgCl_2$).[72, 73, 96] Thus, it is possible that the NH_3 absorption phenomena positively affects on the reaction between NH_3 and LiH.

1.5 Thermodynamics

Some materials such as halides and borohydrides absorb ammonia and ammine complexes as thermodynamically stable phase as described above. To understand the reaction details, thermodynamics is important.

The standard Gibbs' energy of reaction ΔG is written by follows,

$$\Delta G = \Delta H - T\Delta S, \quad (1.22)$$

$$\Delta S = \Delta S^0 - R\ln(p_{pro}/p_0), \quad (1.23)$$

where T is the reaction temperature (K), ΔH is the standard enthalpy of reaction (kJ/mol), ΔS is the entropy of reaction (J/mol・K), ΔS^0 is the the standard entropy of reaction (J/mol・K), p_{pro} is the partial pressure of produced gas (kPa), p_0 is the standard pressure (101.325 kPa). In $\Delta G = 0$, the condition is thermodynamically equilibrium state, and the NH_3 absorption and desorption reaction simultaneously proceed. In $\Delta G < 0$, reactions proceed spontaneously. In $\Delta G > 0$, reactions does not proceed spontaneously. When ΔH is negative value for the absorption reaction of the above equation, it exothermically proceeds. In the NH_3 desorption process, increase in temperature or decrease in partial pressure of gaseous products are required to satisfy $\Delta G < 0$ due to positive ΔH value. Thus, the reaction is controlled by temperature and pressure.

The Van't Hoff equation is obtained by using the above-mentioned p_{eq} and thermodynamic parameters (ΔH, ΔS) as follows,

$$\ln p_{eq} = -\Delta H/RT + \Delta S/R, \quad (1.24)$$

This equation also shows the temperature dependence of the p_{eq}. ΔH and ΔS are estimated from the slope and intercept of the straight line plotting $\ln p_{eq}$ and reciprocal of T.

As mentioned above, the equilibrium state of the ammonia absorption is determined by temperature and ammonia pressure. Generally, the pessure-composition-isothermal (PCI) measurements is useful technique to understand thermodynamic properties of the materials. As example, PCI curve of lithium chloride (LiCl) as a typical ammonia absorbing material at 20 °C is shown in Figure 1.8.[73]

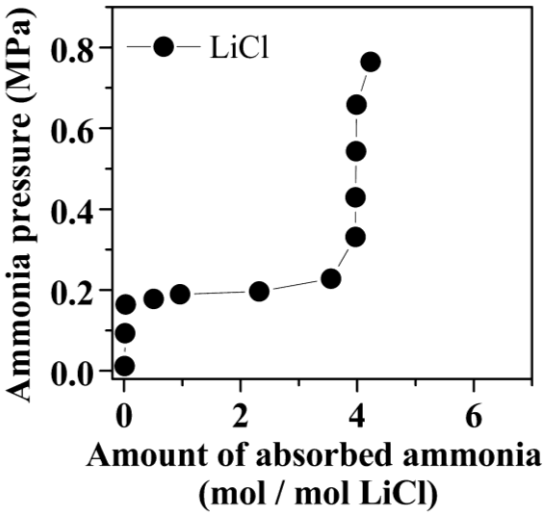

Figure 1.8 The NH_3 absorption property of LiCl at 20 °C

The *x* and *y* axes are the amount of absorbed NH_3 for 1 mol of LiCl and the ammonia pressure, respectively. With increase in the introduced NH_3, only pressure in the experimental system rises below 178 kPa. The ammonia absorption starts at 178 kPa, the pressure is constant value during the increase in the amount absorbed NH_3 from 0 to 2, indicating that the ammonia absorbing reaction proceeds as follows,

$$LiCl + 2NH_3 \leftrightarrows Li(NH_3)_2Cl. \quad (1.25)$$

This pressure is generally called plateau pressure and represented by the symbol of p_{eq} as described above. In this plateau region, since the number of component

C and phase *P* respectively correspond to 2 and 3, the degree of freedom *F* is estimated for the NH_3 absorption reaction from the Gibbs' phase rule as follows,

$$F = C\text{-}P\text{+}2 = 2\text{-}3\text{+}2 = 1. \quad (1.26)$$

Therefore, only one parameter among temperature, pressure, and the amount of absorbed ammonia can be chosen freely, for instance, when a certain temperature is selected, the amount of absorbed ammonia and pressure are uniquely determined. Thus, when the plateau region is observed in the PCI measurements, two phases, which are thermodynamically different stable phases, coexist. In the higher pressure than the plateau pressure, the pressure is simply increased without some reactions. As another example, the PCI curve of sodium borohydride ($NaBH_4$), which reveals characteristic features differently from typical ammonia absorbing materials, as shown in Figure 1.4.[73] The plateau region appears at 93 kPa, and 2 mol of NH_3 is absorbed in $NaBH_4$. In the higher pressure than the plateau pressure, the amount of absorbed ammonia continuously increases with the increase in the ammonia pressure. Assuming that influence of kinetics is negligible, these results indicate that the ammonia absorption state is continuously changed thermodynamically like solid and liquid solution, resulting in a slope-like profile.

1.6 Kinetics

As mentioned in previous section, the reaction conditions and yield are determined by thermodynamic properties of the reactions. In this section, it is described about the kinetics to reach thermodynamic equilibrium. The reaction kinetics is increased with the increase of the reaction rate constant $k(T)$, and it is expressed by the following equation,

$$k(T) = A\exp(-E_a/RT), \quad (1.27)$$

where A is the frequency factor, E_a is the activation energy, R is gas constant, and T is the reaction temperature. Equation (1.27) indicates that reaction rate can be improved by the increase of A and T, or the decrease of E_a. For instance, it is possible to increase A by reacting under higher pressure in the gas-solid reaction. When the reaction is operated under higher temperature, the reaction rate is improved. To decrease E_a, suitable catalysts with considering the rate-determining step are generally used. To control the kinetic properties, it is most important to understand the detailed reaction processes (rate-determining step), which are elementary reactions included in the reaction. Here, the reaction process in the hydrogen absorption reaction of the hydrogen storage alloy which is a typical solid-gas phase reaction is thought as example. The reaction is described as follows,

$$M + H_2 \leftrightarrows MH_2, \quad (1.28)$$

where M is mainly composed of transition metals such as $LaNi_5$, TiFe, and Mg_2Ni.[97-99] The reaction proceeds by five intermediate partial processes as below:[100]

(i) Physisorption of hydrogen molecules on the surface of alloy;

(ii) Dissociation of hydrogen molecules to hydrogen atoms and chemical adsorption hydrogen atoms on the surface of alloy;
(iii) Immigration of hydrogen atoms from the surface into alloy;
(iv) Diffusion of hydrogen atoms in alloy;
(v) Formation of alloy hydrides.

When (ii) is rate-determining process, dissociation of hydrogen molecules can be promoted by the addition of a hydrogen dissociation catalyst such as Pt. The catalytic effect on dissociation of hydrogen molecules is understood to appear because *d* electrons in noble metals and transition metals interact with hydrogen molecules and reduce the E_a of the dissociation process. Actually, the hydrogen desorption reaction of hydrogen storage alloy proceeds relatively fast because it often contains transition metal. In addition, when (iv) is the rate-determining step, the decrease of the size of reactants is effective to improve the kinetics because the diffusion distance of atoms is shortened.

References

1. Kansai Electric Power Co., https://www.kepco.co.jp/energy_supply/energy/nowenergy/world_energy.html.
2. Toshiba Energy Systems and Solutions Co., https://www.toshiba-energy.com/hydrogen/.
3. B. Sakintuna, F. Lamari-Darkrim and M. Hirscher, *International Journal of Hydrogen Energy*, 2007, **32**, 1121-1140.
4. S.-W. Cho, C.-S. Han, C.-N. Park and E. Akiba, *Journal of Alloys and Compounds*, 1999, **288**, 294-298.
5. N. Hanada, T. Ichikawa, S. Hino and H. Fujii, *Journal of Alloys and Compounds*, 2006, **420**, 46-49.
6. L. Schlapbach and A. Züttel, in *Materials for Sustainable Energy*, DOI: 10.1142/9789814317665_0038, pp. 265-270.
7. A. Züttel, P. Wenger, S. Rentsch, P. Sudan, P. Mauron and C. Emmenegger, *Journal of Power Sources*, 2003, **118**, 1-7.
8. R. J. Keaton, J. M. Blacquiere and R. T. Baker, *Journal of the American Chemical Society*, 2007, **129**, 1844-1845.
9. G. Sandrock, K. Gross and G. Thomas, *Journal of Alloys and Compounds*, 2002, **339**, 299-308.
10. A. C. Dillon and M. J. Heben, *Applied Physics A*, 2001, **72**, 133-142.
11. F. L. Darkrim, P. Malbrunot and G. P. Tartaglia, *International Journal of Hydrogen Energy*, 2002, **27**, 193-202.
12. H. Miyaoka, T. Ichikawa, S. Isobe and H. Fujii, *Physica B: Condensed Matter*, 2006, **383**, 51-52.
13. A. Klerke, C. H. Christensen, J. K. Nørskov and T. Vegge, *Journal of Materials Chemistry*, 2008, **18**, 2304-2310.
14. C. H. Christensen, T. Johannessen, R. Z. Sørensen and J. K. Nørskov, *Catalysis Today*, 2006, **111**, 140-144.
15. A. Valera-Medina, H. Xiao, M. Owen-Jones, W. I. F. David and P. J. Bowen, *Progress in Energy and Combustion Science*, 2018, **69**, 63-102.
16. L. Green, *International Journal of Hydrogen Energy*, 1982, **7**, 355-359.
17. D. Miura and T. Tezuka, *Energy*, 2014, **68**, 428-436.
18. NIST, *https://webbook.nist.gov/chemistry/*.

19. T. Brown, https://ammoniaindustry.com/ammonia-technology-portfolio-optimize-for-energy-efficiency-and-carbon-efficiency/.
20. SIP, https://www.jst.go.jp/sip/k04.html.
21. F. Besenbacher, I. Chorkendorff, B. S. Clausen, B. Hammer, A. M. Molenbroek, J. K. Nørskov and I. Stensgaard, *Science*, 1998, **279**, 1913.
22. Y. Matsumura and T. Nakamori, *Applied Catalysis A: General*, 2004, **258**, 107-114.
23. D. S. Newsome, *Catalysis Reviews*, 1980, **21**, 275-318.
24. H. Bohlbro and M. Jørgensen, *Chem Eng World*, 1970, **5**, 46-49.
25. G. v. O. F. Haber, *Zeitschrift für anorganische Chemie*, 1905, **44**, 341-378.
26. A. Vojvodic, A. J. Medford, F. Studt, F. Abild-Pedersen, T. S. Khan, T. Bligaard and J. K. Nørskov, *Chemical Physics Letters*, 2014, **598**, 108-112.
27. T. Brown, http://www.ammoniaenergy.org/green-ammonia-demonstration-plants-now-operational-in-oxford-and-fukushima/.
28. T. Brown, http://www.ammoniaenergy.org/ocps-plans-for-green-ammonia-and-an-african-institute-for-solar-ammonia/.
29. T. Brown, https://ammoniaindustry.com/yara-solar-ammonia-pilot-plant-for-start-up-in-2019/.
30. T. Brown, https://ammoniaindustry.com/green-ammonia-demonstration-plant-in-the-netherlands/.
31. T. Brown, https://ammoniaindustry.com/siemens-gamesa-plans-green-ammonia-pilot-plant-in-denmark/.
32. R. F. Service, *Science*, 2018, **361**, 120-123.
33. S. F. Yin, B. Q. Xu, X. P. Zhou and C. T. Au, *Applied Catalysis A: General*, 2004, **277**, 1-9.
34. S.-F. Yin, Q.-H. Zhang, B.-Q. Xu, W.-X. Zhu, C.-F. Ng and C.-T. Au, *Journal of Catalysis*, 2004, **224**, 384-396.
35. A. S. Chellappa, C. M. Fischer and W. J. Thomson, *Applied Catalysis A: General*, 2002, **227**, 231-240.
36. K. Hashimoto and N. Toukai, *Journal of Molecular Catalysis A: Chemical*, 2000, **161**, 171-178.
37. M. C. J. Bradford, P. E. Fanning and M. A. Vannice, *Journal of Catalysis*, 1997, **172**, 479-484.
38. F. Hayashi, Y. Toda, Y. Kanie, M. Kitano, Y. Inoue, T. Yokoyama, M. Hara and H. Hosono, *Chemical Science*, 2013, **4**, 3124-3130.

39. S. Murata and K.-i. Aika, *Journal of Catalysis*, 1992, **136**, 118-125.
40. A.-H. Lu, J.-J. Nitz, M. Comotti, C. Weidenthaler, K. Schlichte, C. W. Lehmann, O. Terasaki and F. Schüth, *Journal of the American Chemical Society*, 2010, **132**, 14152-14162.
41. M. E. E. Abashar, Y. S. Al-Sughair and I. S. Al-Mutaz, *Applied Catalysis A: General*, 2002, **236**, 35-53.
42. H. Inokawa, T. Ichikawa and H. Miyaoka, *Applied Catalysis A: General*, 2015, **491**, 184-188.
43. N. Hanada, S. Hino, T. Ichikawa, H. Suzuki, K. Takai and Y. Kojima, *Chemical Communications*, 2010, **46**, 7775-7777.
44. D. J. Little, I. I. I. M. R. Smith and T. W. Hamann, *Energy & Environmental Science*, 2015, **8**, 2775-2781.
45. K. Goshome, T. Yamada, H. Miyaoka, T. Ichikawa and Y. Kojima, *International Journal of Hydrogen Energy*, 2016, **41**, 14529-14534.
46. B. X. Dong, T. Ichikawa, N. Hanada, S. Hino and Y. Kojima, *Journal of Alloys and Compounds*, 2011, **509**, S891-S894.
47. F. Ephraim, *Berichte der deutschen chemischen Gesellschaft*, 1912, **45**, 1322-1331.
48. W. H. W Biltz, *Z. Anorg. Allgem. Chem*, 1923, **127**, 1– 33.
49. W. a. H. Biltz, G. F., *Z. Anorg. Allg. Chem.*, 1923, **129**, 161– 175.
50. Y. Guo, G. Xia, Y. Zhu, L. Gao and X. Yu, *Chemical Communications*, 2010, **46**, 2599-2601.
51. X. Zheng, G. Wu, W. Li, Z. Xiong, T. He, J. Guo, H. Chen and P. Chen, *Energy & Environmental Science*, 2011, **4**, 3593-3600.
52. G. Soloveichik, J.-H. Her, P. W. Stephens, Y. Gao, J. Rijssenbeek, M. Andrus and J. C. Zhao, *Inorganic Chemistry*, 2008, **47**, 4290-4298.
53. Y. Yang, Y. Liu, Y. Li, M. Gao and H. Pan, *Chemistry – An Asian Journal*, 2013, **8**, 476-481.
54. H. Chu, G. Wu, Z. Xiong, J. Guo, T. He and P. Chen, *Chemistry of Materials*, 2010, **22**, 6021-6028.
55. Y. Guo, Y. Jiang, G. Xia and X. Yu, *Chemical Communications*, 2012, **48**, 4408-4410.
56. Y. Guo, H. Wu, W. Zhou and X. Yu, *Journal of the American Chemical Society*, 2011, **133**, 4690-4693.

57. L. H. Jepsen, M. B. Ley, Y. Filinchuk, F. Besenbacher and T. R. Jensen, *ChemSusChem*, 2015, **8**, 1452-1463.
58. F. Yuan, Q. Gu, X. Chen, Y. Tan, Y. Guo and X. Yu, *Chemistry of Materials*, 2012, **24**, 3370-3379.
59. Z. Tang, F. Yuan, Q. Gu, Y. Tan, X. Chen, C. M. Jensen and X. Yu, *Acta Materialia*, 2013, **61**, 3110-3119.
60. F. Yuan, Q. Gu, Y. Guo, W. Sun, X. Chen and X. Yu, *Journal of Materials Chemistry*, 2012, **22**, 1061-1068.
61. J. Huang, Y. Tan, Q. Gu, L. Ouyang, X. Yu and M. Zhu, *Journal of Materials Chemistry A*, 2015, **3**, 5299-5304.
62. Y. Yang, Y. Liu, H. Wu, W. Zhou, M. Gao and H. Pan, *Physical Chemistry Chemical Physics*, 2014, **16**, 135-143.
63. E. A. Sullivan and S. Johnson, *The Journal of Physical Chemistry*, 1959, **63**, 233-238.
64. S. R. Johnson, W. I. F. David, D. M. Royse, M. Sommariva, C. Y. Tang, F. P. A. Fabbiani, M. O. Jones and P. P. Edwards, *Chemistry – An Asian Journal*, 2009, **4**, 849-854.
65. R. Custelcean and J. E. Jackson, *Chemical Reviews*, 2001, **101**, 1963-1980.
66. H. Miyaoka, H. Miyaoka, T. Ichikawa, T. Ichikawa and Y. Kojima, *International Journal of Hydrogen Energy*, 2018, **43**, 14486-14492.
67. S. Crolius, *http://www.ammoniaenergy.org/csiro-demonstrates-ammonia-to-hydrogen-fueling-system/*, 2018.
68. L. C. Yi and A. Ken-ichi, *Bulletin of the Chemical Society of Japan*, 2004, **77**, 123-131.
69. R. Halseid, P. J. S. Vie and R. Tunold, *Journal of Power Sources*, 2006, **154**, 343-350.
70. ISO14687-2.
71. C. H. Christensen, R. Z. Sørensen, T. Johannessen, U. J. Quaade, K. Honkala, T. D. Elmøe, R. Køhler and J. K. Nørskov, *Journal of Materials Chemistry*, 2005, **15**, 4106-4108.
72. R. Z. Sørensen, J. S. Hummelshøj, A. Klerke, J. B. Reves, T. Vegge, J. K. Nørskov and C. H. Christensen, *Journal of the American Chemical Society*, 2008, **130**, 8660-8668.
73. T. Aoki, T. Ichikawa, H. Miyaoka and Y. Kojima, *The Journal of Physical Chemistry C*, 2014, **118**, 18412-18416.

74. T. Zhang, H. Miyaoka, H. Miyaoka, T. Ichikawa and Y. Kojima, *ACS Applied Energy Materials*, 2018, **1**, 232-242.
75. F. W. Dafert and R. Miklauz, *Monatshefte für Chemie und verwandte Teile anderer Wissenschaften*, 1910, **31**, 981-996.
76. O. Ruff and H. Goeres, *Chem. Ber.*, 1910, **44**, 502-506.
77. P. Chen, Z. Xiong, J. Luo, J. Lin and K. L. Tan, *Nature*, 2002, **420**, 302.
78. P. Chen, Z. Xiong, J. Luo, J. Lin and K. L. Tan, *The Journal of Physical Chemistry B*, 2003, **107**, 10967-10970.
79. C. M. Araújo, A. Blomqvist, R. H. Scheicher, P. Chen and R. Ahuja, *Physical Review B*, 2009, **79**, 172101.
80. W. Li, G. Wu, Z. Xiong, Y. P. Feng and P. Chen, *Physical Chemistry Chemical Physics*, 2012, **14**, 1596-1606.
81. P. Chen and M. Zhu, *Materials Today*, 2008, **11**, 36-43.
82. M. W. Chase, Jr., *J. Phys. Chem. Ref. Data*, Monograph 1998, **9**, 1.
83. S. Isobe, T. Ichikawa, S. Hino and H. Fujii, *The Journal of Physical Chemistry B*, 2005, **109**, 14855-14858.
84. T. Ichikawa, N. Hanada, S. Isobe, H. Leng and H. Fujii, *The Journal of Physical Chemistry B*, 2004, **108**, 7887-7892.
85. H. Y. Leng, T. Ichikawa, S. Hino and H. Fujii, *Journal of Alloys and Compounds*, 2008, **463**, 462-465.
86. H. Yamamoto, H. Miyaoka, S. Hino, H. Nakanishi, T. Ichikawa and Y. Kojima, *International Journal of Hydrogen Energy*, 2009, **34**, 9760-9764.
87. H. Y. Leng, T. Ichikawa, S. Hino, N. Hanada, S. Isobe and H. Fujii, *Journal of Power Sources*, 2006, **156**, 166-170.
88. S. Hino, N. Ogita, M. Udagawa, T. Ichikawa and Y. Kojima, *Journal of Applied Physics*, 2009, **105**, 023527.
89. D. R. Lide, *CRC Handbook of Chemistry and Physics*, CRC Press, New York, 84th edn, 2003–2004
90. H. Miyaoka, K. Tange, H. Yamamoto, S. Hino, T. Ichikawa and Y. Kojima, *International Journal of Hydrogen Energy*, 2015, **40**, 14911-14915.
91. Y. Kojima, K. Tange, S. Hino, S. Isobe, M. Tsubota, K. Nakamura, M. Nakatake, H. Miyaoka, H. Yamamoto and T. Ichikawa, *Journal of Materials Research*, 2011, **24**, 2185-2190.
92. B.-X. Dong, L. Song, Y.-L. Teng, J. Ge and S.-Y. Zhang, *International Journal of Hydrogen Energy*, 2014, **39**, 13838-13843.

93. Y.-L. Teng, T. Ichikawa, H. Miyaoka and Y. Kojima, *Chemical Communications*, 2011, **47**, 12227-12229.
94. H. Miyaoka, H. Fujii, H. Yamamoto, S. Hino, H. Nakanishi, T. Ichikawa and Y. Kojima, *International Journal of Hydrogen Energy*, 2012, **37**, 16025-16030.
95. B.-X. Dong, L.-T. Chen, Y.-L. Teng, J.-J. Gao and H. Tian, *Journal of Materials Science*, 2016, **51**, 911-916.
96. M. M. Szczęśniak, Z. Latajka, P. Piecuch, H. Ratajczak, W. J. Orville-Thomas and C. N. R. Rao, *Chemical Physics*, 1985, **94**, 55-63.
97. C. N. Park and J. Y. Lee, *Journal of the Less Common Metals*, 1982, **83**, 39-48.
98. J. J. Reilly and R. H. Wiswall, *Inorganic Chemistry*, 1974, **13**, 218-222.
99. J. J. Reilly and R. H. Wiswall, *Inorganic Chemistry*, 1968, **7**, 2254-2256.
100. M. Martin, C. Gommel, C. Borkhart and E. Fromm, *Journal of Alloys and Compounds*, 1996, **238**, 193-201.

2 Purpose

To effectively utilize ammonia (NH_3) as an energy or a hydrogen (H_2) carrier, the NH_3 absorbing materials and H_2 storage system are investigated and discussed as fundamental research about the following two topics,

(1) Spectroscopic analyses for NH_3 absorbing process of $NaBH_4$,

(2) Catalytic effects of NH_3 absorbing materials on H_2 generation of NH_3-LiH system.

(1) Spectroscopic analyses for NH_3 absorbing process of $NaBH_4$

The NH_3 absorbing materials are attractive as H_2 (or NH_3) storage materials and/or functional materials for establishing the safety devices. Among them, we focused on sodium borohydride ($NaBH_4$) as an NH_3 absorbing material to understand the relation of the NH_3 absorbed state and chemical state in the NH_3 absorption process. $NaBH_4$ revealed characteristic properties differently from the other materials because the formation of liquid solution between NH_3 and $NaBH_4$ is expected. However, the detailed reaction process has not been understood yet due to the difficulty of characterization under NH_3 atmosphere without exposing air.

In this work, the NH_3 absorbing process of $NaBH_4$ was investigated in further details by using operando nuclear magnetic resonance spectroscopy and Fourier transform infrared spectroscopy under NH_3 atmosphere. And, thermodynamic analysis based on solution theory for the NH_3 pressure-composition isothermal curve was performed to discuss and understand the phase variation and the absorption behavior of the $NaBH_4$-NH_3 system.

(2) Catalytic effects of NH_3 absorbing materials on H_2 generation of NH_3-LiH system

The NH_3-LiH system is expected as a H_2 storage system because of its high gravimetric and volumetric hydrogen density. However, the H_2 desorption reaction proceeds slowly, and the kinetic improvement is required. So far, titanium chloride ($TiCl_3$) is the most effective as a catalyst. However, in the process of the sample preparation, LiH reacted with $TiCl_3$ and change to other materials as described in introduction.

In this work, firstly, the additive effects of titanium (Ti), titanium hydride (TiH_2), and lithium chloride (LiCl) are investigated based on the previous research. Furthermore, the additive effects of the NH_3 absorbing materials such as $LiBH_4$ and $NaBH_4$ for the H_2 generation reaction of the NH_3-LiH system were systematically investigated to understand the catalytic process on this system.

3 Experiments

3.1 Materials

Experiments were carried out by the use of materials shown in Table 3.1. Since these materials are active to oxygen or water in the air and easily change to oxides and hydroxides, all the samples were handled in a glovebox purified by a gas recycling purification system (MP-P-60W, Miwa MFG Co., Ltd.) to minimize influence of oxygen and water in the air.

Table 3.1 The information of materials used for experiments

Material (Chemical formula)	Purity (%)	Company
Lithium hydride (LiH)	99.4	Alfa Aesar
Titanium (Ti)	99.9	Rare metallic
Titanium(II) hydride (TiH_2)	98	Sigma Aldrich
Lithium chloride (LiCl)	99.99	Sigma Aldrich
Lithium borohydride ($LiBH_4$)	95	Sigma Aldrich
Sodium borohydride ($NaBH_4$) for NH_3-LiH experiment	98	Sigma Aldrich
Sodium borohydride ($NaBH_4$) for NMR and IR experiment	99.99	Sigma Aldrich

3.2 Pressure-Composition isotherms

The NH_3 Pressure-Composition isothermal (PCI) measurements are a technique to know the relationship between the NH_3 pressure and the absorbed amount of NH_3 at an arbitrary temperature. There are two methods for PCI measurements, named gravimetric and volumetric (Sieverts') methods. In the gravimetric and volumetric methods, the composition at each pressure is evaluated from the change in weight and pressure, respectively. In this study, NH_3 PCI measurements were carried out by the volumetric method. Figure 3.1 shows a schematic diagram of the volumetric PCI measurement system.

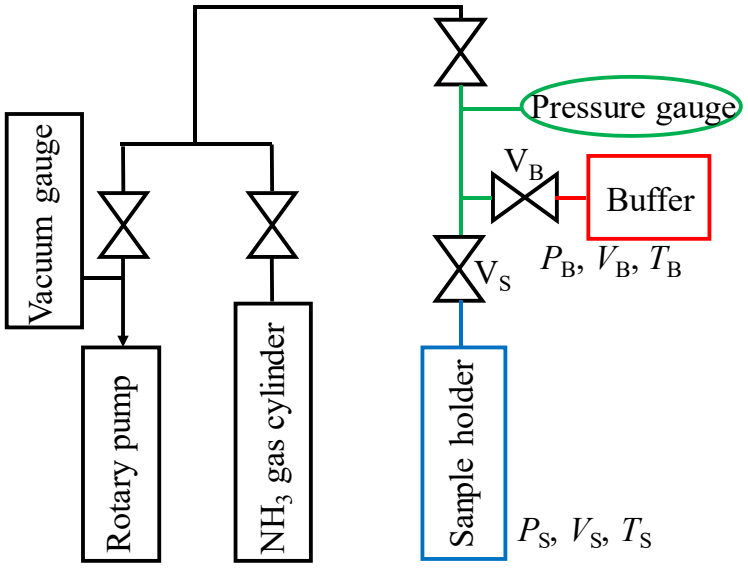

Figure 3.1 Schematic diagram of the volumetric PCI measurement system

The apparatus is composed of a buffer and a sample holder, and their volume is denoted as $V_{B(\text{buffer})}$ and $V_{S(\text{sample holder})}$, respectively. Here, the buffer indicates the green and red area in Figure 3.1 and the valve V_B is ordinary open. When the density of NH_3 is written by $d(P, T)$ in the pressure P and the temperature T, the

amount of NH_3 gas n in the initial state could be written as follows,

$$n = d(P_B, T_B)V_B + d(P_S, T_S)V_S. \quad (3.1)$$

Here, the pressure and temperature of the buffer and sample holder are denoted as P_B, P_S, T_B, and T_S, respectively.

In the initial state, P_B is higher than P_S. When the valve V_S is opened in this state, the amount of NH_3 gas and each pressure change to n', P_B', P_S', and the following equation could be written,

$$n' = d(P_B', T_B)V_B + d(P_S', T_S)V_S. \quad (3.2)$$

At this time, P_B' is equal to P_S', and the amount of ammonia contributing to the NH_3 absorption reaction could be estimated from n-n'. By the repeat of the above procedures, PCI curves can be obtained.

Procedure

The PCI measurements were performed for $NaBH_4$ at 0 and 20 °C. In the measurement at 0 °C, the hand-made apparatus is used, and the image is shown in Figure 3.1. The volume of green, red, and blue area, which are related to the PCI measurements, are 14.8, 49.6, and 9.8 cm^3, respectively. The temperature of the sample holder is kept 0 °C by ice water. The measurements were performed for 1 mmol of $NaBH_4$ in the pressure region from 0.002 to 428 kPa. The lower pressure is vacuumed by the rotary pump (ULVAC, GLD-051) and monitored by the Pirani vacuum gauge (ULVAC, GP-2A). The higher pressure is monitored by pressure gauge (Druck, DPI280) and the maximum value is almost the liquefied pressure of NH_3 (431 kPa) at 0 °C.[1] When the pressure value did not change within 1 kPa for 5 min after the introduction of NH_3 gas, the system was judged to be an equilibrium pressure.

The commercial apparatus is used for the measurement at 20 °C. 30 mg of $NaBH_4$ is introduced into a sample holder, and the measurement is performed in the pressure range from 0.08 to 705 kPa. This maximum value was determined to prevent the liquefaction of NH_3 gas which is for the introduction into sample holder. When the pressure change was within 1 kPa for 15 min, the pressure was regarded as the equilibrium pressure.

3.3. Operando Fourier transform infrared spectroscopy

Fourier transform infrared (FT-IR) spectroscopy can be used for solid, liquid, and gas phases. By using FT-IR, chemical bonds such as functional groups in samples are able to be qualitatively and quantitatively analyzed.

There are two types of infrared spectrophotometers: dispersed type and Fourier transform type. The difference of them is the optical system. In the dispersed type, the ray after passing through the sample is distributed by the diffraction grating, and each wavelength is sequentially detected. In the Fourier transform type, interferometers are used to detect all wavelengths at the same time. Then, Fourier transform is performed to separate each wavelength component. In this work, Fourier transform type is used.

When rays are irradiated on a molecule and Bohr's quantum condition is satisfied, a part of the ray energy is transferred to a molecule. The molecule absorbs the energy difference between the two quantum states by the excitation from one energy state to a higher energy state. The energies related to molecules could be classified into vibrational, rotational and translational energies. Infrared absorption is mainly due to transitions between vibration energy. Therefore, the infrared absorption spectrum is one type of vibration spectrum.

Atoms in a molecule are chemically bonded, and can be represented by a model composed of two atoms connected by a spring as shown in Figure 3.2.

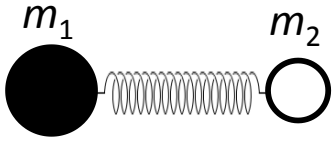

Figure 3.2 The model of molecule composed of two atoms connected by a spring

The frequency of vibration between the two atoms is expressed by the following equation,

$$\nu = \frac{1}{2\pi}\sqrt{\frac{k}{M}}, \quad (3.3)$$

$$M = \frac{m_1 m_2}{m_1 + m_2}, \quad (3.4)$$

where m_1 and m_2 are the masses of the two atoms, and k is spring constant. When the frequency corresponds to the wavelength of infrared rays, the rays are absorbed by molecules. On the other hand, not all molecules absorb infrared rays. Dipole moment occurs when positive and negative charges are generated on individual atoms in a molecule. When the dipole moment of the molecule is changed by vibration, the molecule absorbs infrared ray. Therefore, the infrared is not absorbed for the diatomic molecules such as H_2, O_2, and N_2 because the dipole moment is not changed even if the vibration is happened. The samples used in this study have N-H or B-H bonds and these are infrared active.

Procedure

In this work, the FT-IR measurements were performed to understand the NH_3 absorption state of $NaBH_4$. FT-IR (Spectrum One, Perkin-Elmer) system equipped with diffuse reflection cell were used to observe infrared absorption spectra. Here, the NH_3 absorption and desorption reaction of $NaBH_4$ proceeds reversibly, and the absorbed NH_3 is released without NH_3 pressure. Thus, in order to characterize the NH_3 absorption state of $NaBH_4$, the measurement must be performed under NH_3 pressure. Therefore, the special sample cell, which can be utilized in NH_3 atmosphere without corrosion. Although a commercially available sample cell can change inside atmosphere with our demand, various

raw materials are not resistance to NH_3. In this work, the home-made sample cell by Hydrolab Inc. was used and the image is shown in Figure 3.3. The size of the sample cell is shown in Table 3.2. The sample cell is mainly made from steel use stainless (sus316). The yellow cell wiendow is made from zinc selenide (ZnSe), and the Kalrez o-ring is used for sealing. The available pressure range is from 0.002 to 860 kPa of NH_3 pressure, which is vapor pressure of NH_3 at 20 °C. The samples were measured without dilution. Spectra were recorded at 4 accumulations with 4 cm^{-1} spectral resolution.

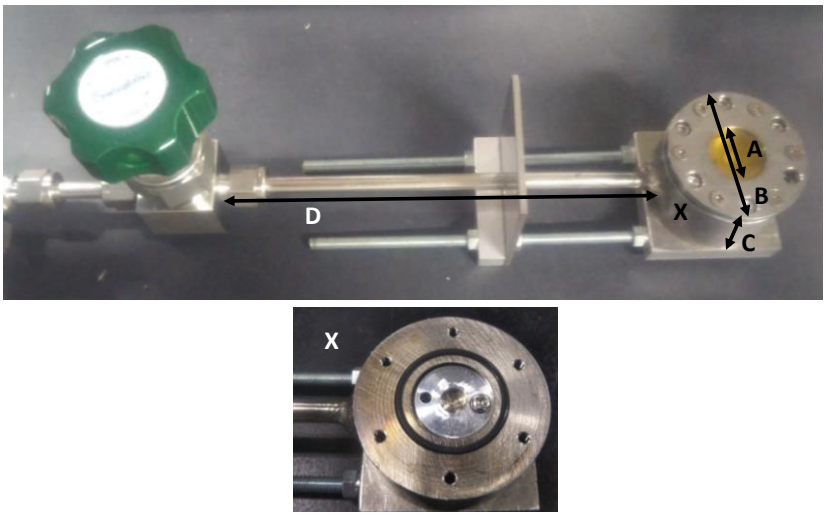

Figure 3.3 The image of the sample cell for FT-IR

Table 3.2 The size of the sample cell for FT-IR in Figure 3.3

Parts	Size (mm)
Window diameter(A)	21.0
Cell diameter(B)	50.0
Cell height(C)	23.3
Length (D)	50.7

3.4 Operando nuclear magnetic resonance spectroscopy

An atom is composed of a nucleus and electrons. Nuclei causes a resonance phenomenon by irradiation of radio waves in magnetic fields. This resonance phenomenon is used for various atoms to analyze their chemical states, and this is named nuclear magnetic resonance (NMR). The nuclear spin in nucleus is the most important for NMR. Protons and neutrons in the nucleus are spinning. In the same nucleus, protons and neutrons form the pairs of spins with other protons in opposite directions. When pairs of spin are formed, the properties of spin are canceled. Number of protons, number of neutrons, spin quantum number *I*, and natural abundance for various nuclei are shown in Table 3.3.

Table 3.3 Number of protons and neutrons, spin quantum number *I*, and natural abundance for various isotopes

Isotope	Number of proton	Number of neutron	Spin	Natural abundance (%)
^{1}H	1	0	1/2	99.985
^{2}H	1	1	1	0.015
^{14}N	7	7	1	99.63
^{15}N	7	8	1/2	0.037
^{23}Na	11	12	3/2	100
^{10}B	5	5	3	19.58
^{11}B	5	6	3/2	80.42
^{16}O	8	8	0	99.74
^{17}O	8	9	5/2	0.037
^{18}O	8	10	0	0.205
^{12}C	6	6	0	98.92
^{13}C	6	7	1/2	1.08

In the case of ^{1}H, ^{15}N, and ^{11}B, I is half-integer due to the odd number for either proton or neutron. In the case of ^{2}H, ^{14}N, and ^{10}B, I is integer due to the odd number for both proton and neutron. In the case of ^{16}O, ^{18}O, and ^{12}C, I is zero due to the even number for both proton and neutron. Here, nucleus like ^{16}O cannot be observed by NMR measurement because I is equal to 0. By the spins of positively charged nucleus, a magnetic moment is generated. In other words, nucleus could be regarded as a small magnet with magnetic field by itself. There is ordinarily no particular orientation for these small magnets, on the other hand, these are oriented in an external magnetic field. The number of this orientation is determined by I. For example, there are 7 orientations in the case of ^{10}B with $I = 3$. In the case of ^{1}H with $I = 1/2$, there are 2 orientations for 1/2, -1/2. For ^{1}H, 2 orientations are parallel and antiparallel to the magnetic field. Here, the parallel is more stable than the antiparallel. The energy in this high and low energy state (E^{+} and E^{-}) are written by the nuclear magnetic moment μ as the following equation,

$$E^{+} = \mu H_0, \tag{3.5}$$

$$E^{-} = -\mu H_0. \tag{3.6}$$

Thus, the difference of energy between the two states ΔE is expressed as follows,

$$\Delta E = E^{+} - E^{-} = 2\mu H_0.$$

This phenomenon is called Zeeman effect. By the irradiation of an electromagnetic wave with the energy of ΔE, the low energy state can be excited to the high energy state. This is the NMR, and the resonance condition is expressed as follows,

$$\Delta E = 2\mu H_0 = h\nu, \tag{3.7}$$

where h is the Planck's constant, and ν is the frequency of the electromagnetic

wave. Therefore, the resonance frequency is expressed as follows,

$$\nu = 2\mu H_0/h. \quad (3.8)$$

The μ for H can be written as follows.

$$\mu = \gamma h/4\pi, \quad (3.9)$$

where γ is gyromagnetic ratio. Therefore, ν can be rewritten as follows,

$$\nu = \gamma H_0/2\pi. \quad (3.10)$$

Here, the resonance of ^{1}H in a magnetic field of 2.35 T is calculated as follows,

$$\nu = \gamma H_0/2\pi = 2.68*10^8\ (T^{-1} \cdot s^{-1})*\ 2.35\ (T)/2/3.14$$

$$= 1.00*10^8\ (s^{-1}) = 100\ (MHz)$$

The wavelength can be estimated by this value of resonance frequency to be about 3 m, thus this is matched with the radio wave region. As mentioned above, NMR measurement can be measured for various nuclei in principle, assuming that the isotope is considered. However, it is difficult to measure some atoms because of the weakness of intensity. The sensitivity S in NMR measurement is expressed as follows,

$$S = I(I+1)\nu^3 N. \quad (3.11)$$

N is the concentration of the nucleus to be measured in the sample. For instance, ^{15}N and ^{17}O are active for NMR in principle. However, the natural abundance is very low about 0.04% for ^{15}N and ^{17}O. Furthermore, it is difficult to measure ^{14}N and ^{18}O, which are the most major isotope in each nucleus, because of I = 0. Therefore, it is difficult to measure these nucleus in nature. On the other hand, S is composed of the intensity and width of a peak, thus, the signal cannot be observed by the broadening of the peak because of the quadrupole nuclear and state of material.

In the above, the magnetic field for magnetic resonance is assumed to be

equal to the external magnetic field. However, the magnetic field for resonance is different from H_0 due to the effect of electrons around nucleus. Electrons shield the nucleus from the external magnetic field. Since this induced magnetic field is proportional to the static magnetic field H_0, and it can be written as σH_0. Thus, it is necessary to apply a magnetic field H_{eff} to obtain the resonance, and H_{eff} is expressed as follows,

$$H_{\mathrm{eff}} = H_0 - \sigma H_0 = (1 - \sigma) H_0. \tag{3.12}$$

σ is shielding constant. Chemical shifts δ are caused by differences in this shielding constant and are expressed by the following equations,

$$\delta\ (\mathrm{ppm}) = (\nu_{\mathrm{sample}} - \nu_{\mathrm{reference}})/\nu_{\mathrm{reference}} \times 10^6, \tag{3.13}$$

where ν_{sample} and $\nu_{\mathrm{reference}}$ are resonance frequency of the sample and reference, respectively. Here, the denominator and numerator in the equation (3.13) are usually expressed by Hz and MHz, therefore, it is multiplied by 10^6 in order to cancel the difference of digit, and δ is expressed by parts per million (ppm). Here, left and right on NMR chart are expressed as Figure 3.4.

As described above, the chemical shift varies by the difference of the shielding which depends on the electron density around the nucleus. For example, polarization caused by differences in electronegativity between atoms, which is named inductive effect, affects chemical shifts. In the case of halides, the electronegativity increases in the order of I, Br, Cl and F. The electron density of the combined atom is decreased and the shielding is decreased. As the result, the peak is shifted to lower magnetic field. Hydrogen bond is also reason for chemical shift. Actually, when the pure liquid with hydrogen bonds between molecules is diluted with an inactive solvent, the proportion of molecules with hydrogen bond gradually decreases and shifts to the higher

magnetic field.[2]

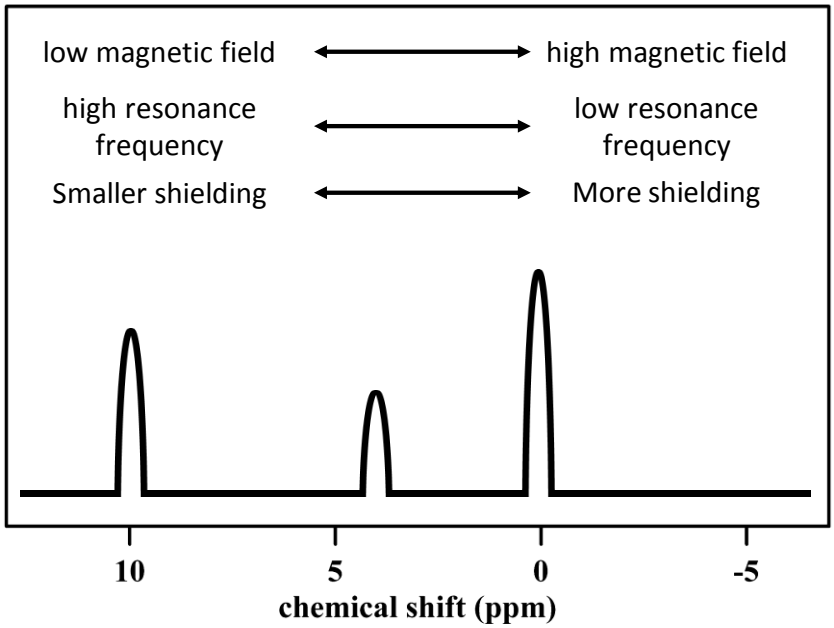

Spin-spin coupling is one of the important information in NMR measurements.[3] Split of signal for hydrogen fluoride (HF) with I=1/2 for both nucleus is thought as an example. When the ^{1}H NMR measurements are performed for HF, the ^{1}H spectrum is affected by the orientation of spin of F. Since the resonance frequency is different between H and F, the spins of F are in the states of 1/2 and -1/2 with the almost same number under the magnetic field for ^{1}H. The nucleus with spin has a property as a small magnet and creates a small magnetic field. Therefore, the fine magnetic field causes the split of the ^{1}H signal into 2 peaks. This split is due to spin-spin coupling with F. In the NMR measurement of ^{19}F, the signal splits into 2 peaks by spin-spin coupling because of I=1/2 in ^{1}H. Here, the NMR spectrum of acetaldehyde (CH_3CHO) is analyzed as follows. The ^{1}H signal of CHO group splits into 4 peaks with the

intensity of 1:3:3:1 because the spin of H in CH_3 group oriented (1/2,1/2,1/2), (1/2,1/2,-1/2), (1/2,-1/2,1/2), (-1/2,1/2,1/2), (1/2,-1/2,-1/2), (-1/2,1/2,-1/2), (-1/2,-1/2,1/2), (-1/2,-1/2,-1/2). For ^1H signal of CH_3 group, the signal split into 2 peaks by the spin-spin coupling of CHO group.

Procedure

^1H and ^{11}B NMR spectra were recorded on a Lambda500 spectrometer (JEOL Co. Ltd.) in a magnetic field of 11.7 T. $NaBH_4$ was packed into High Pressure Valved NMR Tube (S-5-500-HW-HPV-7, Tokyo Chemical Industry Co., Ltd.). This NMR tube can be used from vacuum to 1400 kPa, which is enough wide for the required pressure range of the experiments in this work (0.002~ 689 kPa). Photo of the above NMR tube is shown in Fig 3.5. The size of the NMR tube is shown in Table 3.4, and the volume is 6 cc under the valve. In Figure 3.5-Y, a is perfluoroelastomer o-ring, b is polytetrafluoroethylene (PTFE), c is ethylene tetrafluoro ethylene (ETFE), d is steel use stainless (sus316), and e is perfluoroalkoxy alkane (PFA). c and e are not connected with gas, and the other parts, which connects with NH_3 gas, are resistant to NH_3 gas. Chemical shifts were referenced to chloroform at 7.26 ppm for ^1H and saturated boric acid aqueous solution at 19.49 ppm for ^{11}B. Spectra were acquired with the pulse widths of 1.5–2.0 and 1.75–2.0 μs, and relaxation delays of 5 and 6 s for ^1H and ^{11}B, respectively. The NMR tube were connected to the Sievert-type experimental system which is explained in section 3.2. By using the systems, all the analyses can be conducted with the PCI measurements to know the NH_3 absorption stages. The NMR measurements are repeated by the connection and disconnection of the sample tube.

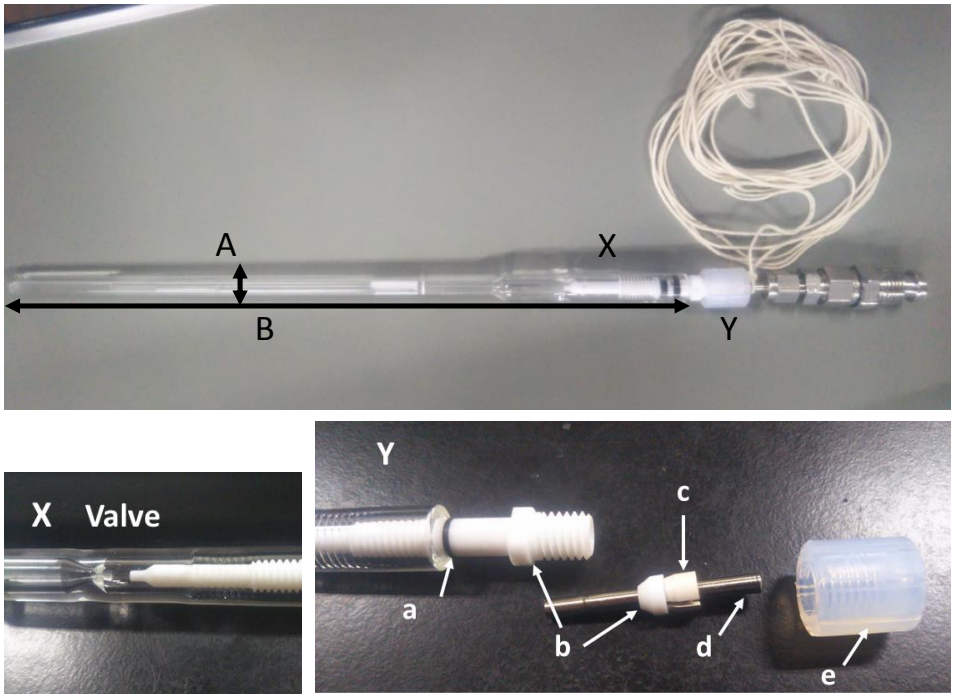

Figure 3.5 The image of the high pressure valved NMR tube

Table 3.4 The size of the NMR tube in Figure 3.5

Parts	Size (mm)
Outside diameter(A)	5.0
Inside diameter(A)	2.2
Thickness of glass	1.4
Length (B)	178.0

3.5 Mechanical ball-milling method

The ball-milling method was used for sample preparation. In the ball-milling, hard balls and solid sample are put into a container, and the container is rotated. Then, mechanical energy, such as impact and grinding, is applied to sample, and crystalline and particle size of samples is decreased. The ball-milling methods are useful to synthesize fine powders, homogeneous mixed state, stable (and metastable) compounds, and alloys. In this research, the planetary ball-milling apparatus as shown in Figure 3.6 is used to disperse additives on surface of solid samples.

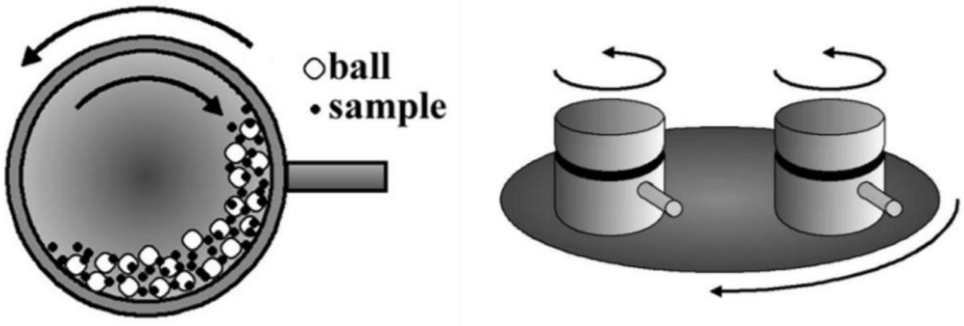

Figure 3.6 The image of the planetary ball-milling

The mixtures of LiH and each additive were milled by using the ball-mill apparatus (P7, Fritsch), and the molar ratio of LiH and additives was chosen to be Li/Ti = 99:1 and LiH/LiCl = 97:3, and the molar ratio of LiH to borohydride, $LiBH_4$ or $NaBH_4$, was also 97:3 to compare the properties of LiH with LiCl.[4] The mixtures in total of 300 mg with 20 steel balls (SUJ-2, 7 mm in diameter) were put into a ball-milling vessel (30 cc, SKD-11, Umetoku Co. Ltd.) in a glovebox (Miwa MFG, MP-P60W), and the ball-milling was performed for 10 h under 0.1 MPa of an Ar atmosphere.

3.6 Powder X-ray diffraction (XRD)

Powder X-ray diffraction is a technique for phase identification, determination of crystal structure, and quantitative analysis of included phases. When X-rays are irradiated on materials, some X-rays penetrate, and some X-rays are scattered by electrons of atoms in materials. Here, in the scattered X-rays, there are elastically scattered X-rays with the same energy as irradiated X-rays and inelastically scattered X-rays with the different energy from irradiated X-rays. In X-ray diffraction measurements, elastically scattered X-ray is analyzed. X-rays are electromagnetic waves and have wave properties. The scattered X-rays from materials are waves with different phases in an arbitrary direction, therefore, almost all waves interferes and weakened each other. However, in a certain direction, the scattered waves are strengthened by interference in same phase. Figure 3.7 shows a schematic image of X-ray diffraction.

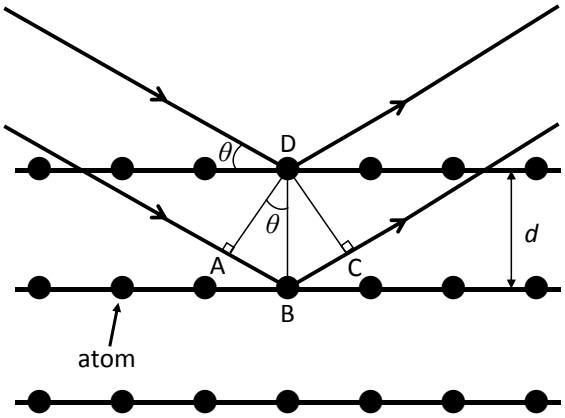

Figure 3.7 Diffraction of X-ray from lattice planes in the crystal

When parallel X-rays 1 and 2 are irradiated at angle θ, the phase is delayed due to AB + BC = $2d\sin\theta$ and scattered. When $2d\sin\theta$ is an integral multiple of the

wavelength of the X-ray, the phases of the waves 1 and 2 match and strengthen each other. Thus, the condition for the diffraction is expressed as follows,

$$2d\sin\theta = n\lambda. \quad (3.14)$$

Here, n is an integer and λ is the wavelength of the X-ray. This equation is known as Bragg's law. The X-ray diffraction pattern is unique to materials, therefore, the crystal structure can be determined by analyzing the XRD pattern.

Procedure

In this work, phases identification of all the samples were performed by the powder XRD measurement (Rigaku, RINT-2500V), in which the X-ray source is Cu-Kα (λ=1.54 Å, 40 kV and 200 mA). Each sample was spread and fixed on the glass plate with high vacuum grease (APIEZON®, H type, M&I Materials Ltd) and covered with polyimide sheet (Kapton®, Du Pont-Toray Co. Ltd, a 7.5 μm thickness) to avoid the oxidation (see Figure 3.8). The obtained XRD patterns are analyzed by the PDXL software with powder diffractions files (PDF) in the database.

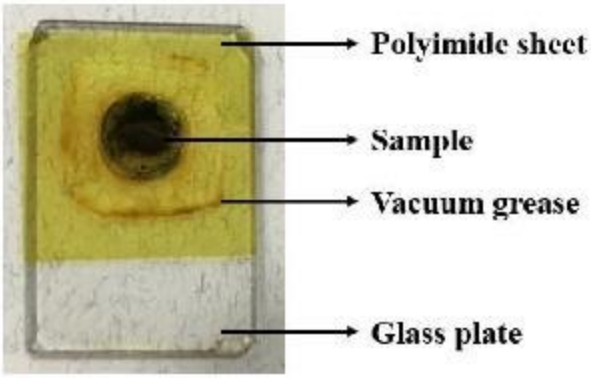

Figure 3.8 Sample preparations for XRD measurements

3.7 Evaluation of reaction yield for LiH-NH_3 system

To investigate effects of additives for the reaction between LiH and NH_3, the following gravimetric method is used. The above reaction is carried out by using the apparatus shown in Figure 3.1. First, all the samples were weighed so as to include 14 mg of LiH in the sample, and it was packed into about 10 cc of reactor, where the accurate reactor volume was estimated before the experiments. Then, the reactor was connected to a Sieverts type apparatus for the reaction. The inside of the reactor was purged by repeats of vacuum using a rotary pump and an Ar filling, and the valve V_S was closed. The H_2 generation by the reaction between each LiH with additive and NH_3 was carried out with a 1:1 molar ratio under 0.45 and 0.10 MPa of NH_3 pressure at room temperature for 1, 12, and 24 h. The reactor volume was adjusted by using a buffer to keep the weight of LiH and the NH_3/LiH molar ratio at different pressures. After finishing the reaction, the inside of the reactor was evacuated by the rotary pump for 10 min at room temperature. The solid products in the reactor were weighed before and after the reaction to estimate the molar amount of the generated $LiNH_2$ (M_{LiNH2}) from the weight gain. The reaction yield was calculated from the molar amount of LiH used for the experiment (M_{LiH}) and M_{LiNH2} as follows,

$$\text{reaction yield} = M_{LiNH2} / M_{LiH} \quad (3.15)$$

Here, it is reported that LiCl, $LiBH_4$, and $NaBH_4$ absorb NH_3 molecules to form stable ammine complexes. If the unreacted NH_3 could remain in the materials even after the evacuation process for 10 min, the weight gain due to the remaining NH_3 is included in the estimated reaction yield. Thus, the weight change by the reaction between each additive and 0.45 MPa of NH_3 was also measured by the same procedure as the H_2 generation reaction to calibrate the

experimental data and to estimate essential reaction yield of LiH. In addition, the valve equipped with the reactor is manually opened and closed at the start and end of the reaction, respectively, suggesting that the experimental error is essentially large compared with accuracy of pressure gauges and thermocouples. Thus, the dispersion of the results for the LiCl dispersing LiH as the representative sample was statistically estimated as a standard deviation by performing the reaction several times at the same conditions. As a result, it was about ±3%.

References

1. NIST, *https://webbook.nist.gov/chemistry/*.
2. J. W. Akitt and B. E. Mann, *NMR and Chemistry: An introduction to modern NMR spectroscopy*, Crc Press, 2000.
3. The Chemical Society of Japan, *Journal*, 1988.
4. H. Miyaoka, H. Fujii, H. Yamamoto, S. Hino, H. Nakanishi, T. Ichikawa and Y. Kojima, *International Journal of Hydrogen Energy*, 2012, **37**, 16025-16030.

4 Results and Discussion

4.1 Spectroscopic analyses for the NH_3 absorbing process of $NaBH_4$

4.1.1 The NH_3 absorption property of $NaBH_4$

Figure 4.1.1 shows the relationship between the concentration and the vapor pressure of NH_3 at 20 °C.[1, 2]

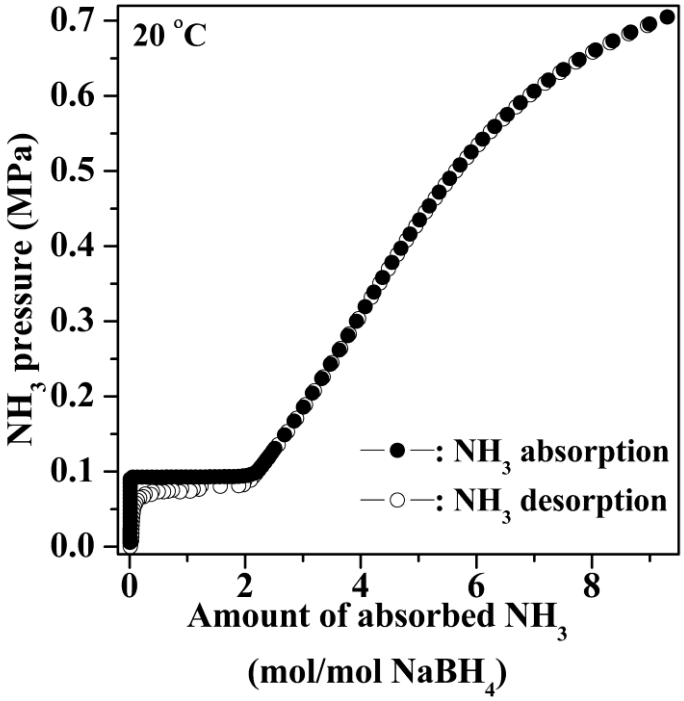

Figure 4.1.1 The PCI result of $NaBH_4$

The closed and opened symbol indicates the NH_3 absorption and desorption process, respectively. The vertical and horizontal axis are NH_3 pressure and the amount of absorbed NH_3 in $NaBH_4$, respectively. When the NH_3 gas is gradually introduced to sample cell with $NaBH_4$ from vacuum, only the NH_3 pressure increases vertically, suggesting that $NaBH_4$ does not react with NH_3.

The plateau appeared at 93 kPa in the PCI curve. In this plateau region, when the NH_3 gas is introduced, the pressure is not changed because $NaBH_4$ absorbs the NH_3 gas. The generated phase should be expressed by chemical equation of $Na(NH_3)_2BH_4$ due to the plateau length corresponding to 2 mol of NH_3. Thus, $NaBH_4$ and $Na(NH_3)_2BH_4$ coexist thermodynamically at the plateau region. The plateau pressure is about one tenth lower than the vapor pressure of liquid NH_3 at 20 °C. During the absorption and desorption cycles, $NaBH_4$ reversibly absorbed and desorbed 2 mol of NH_3, and the equilibrium plateau pressure was not changed.[2] After the plateau region, the vapor pressure was linearly increased with the amount of introducing NH_3. It is expected that the liquid solution of NH_3 and $NaBH_4$ is formed due to the continuous composition variation[1].

4.1.2 Operando ^{11}B NMR measurements under NH_3 pressure

Operando ^{11}B NMR measurements were performed under NH_3 pressure to understand the variation of chemical states during the NH_3 absorption of $NaBH_4$. The measurements were performed at the lower pressure region than the plateau pressure under (a) 9 kPa to (e) 79 kPa of NH_3 as shown in Figure 4.1.2.i. The measurements were performed at the plateau region with $NH_3/NaBH_4$(mol/mol) = (a) 0.3 - (f) 2.0 as shown in Figure 4.1.2.ii. The measurements were performed at the higher pressure than the plateau pressure under (a) 107 kPa to (i) 689 kPa of NH_3 as shown in Figure 4.1.2.iii. The signals of solid $NaBH_4$ and NMR tube are also shown as a reference. The vertical axis of all the profiles are normalized by the highest intensity of the observed signals.

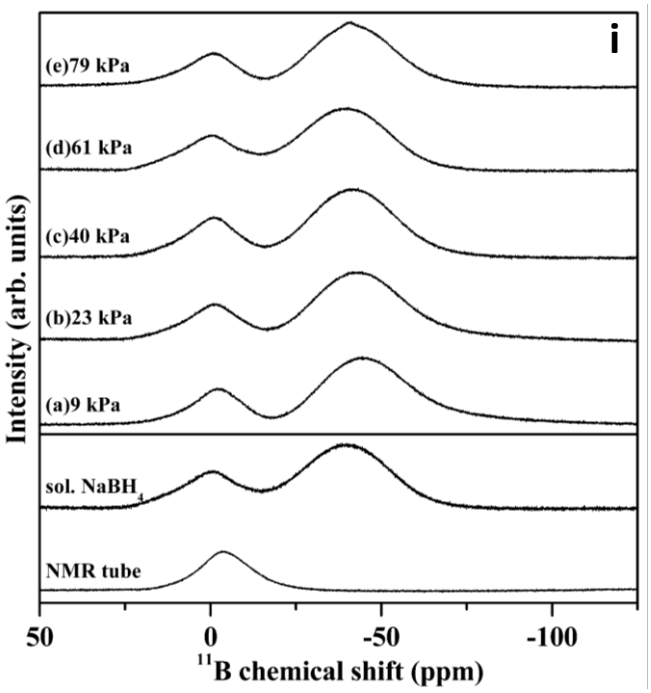

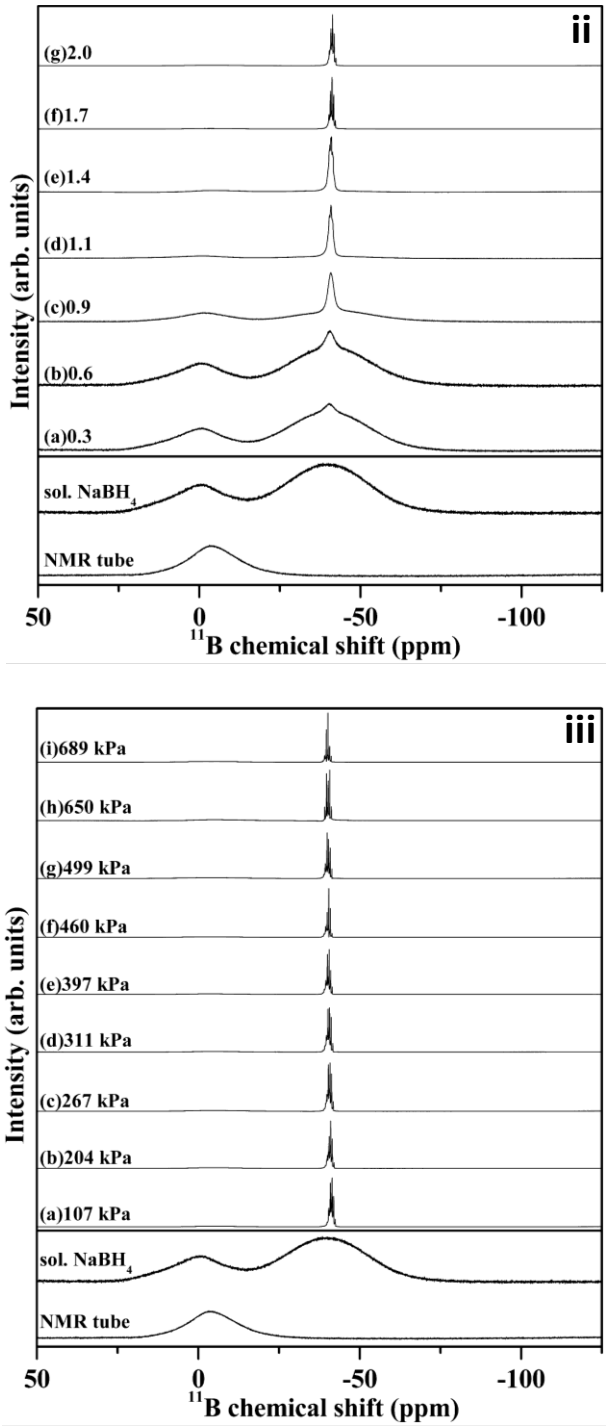

Figure 4.1.2 Operand ^{11}B NMR results for $NaBH_4$ (i) under the plateau pressure (ii) at the plateau region (iii) at the higher pressure than the plateau pressure

borosilicate glass. However, the intensity of NMR tube signal is gradually decreased with the increase in the amount of absorbed NH_3 in $NaBH_4$. This is because the peak intensity of the NMR tube is relatively much lower than the signal around -40.4 ppm from the sample. Actually, when the signals are expanded, the signals of NMR tube are observed with same intensity in all the measurements as shown in Figure 4.1.3.

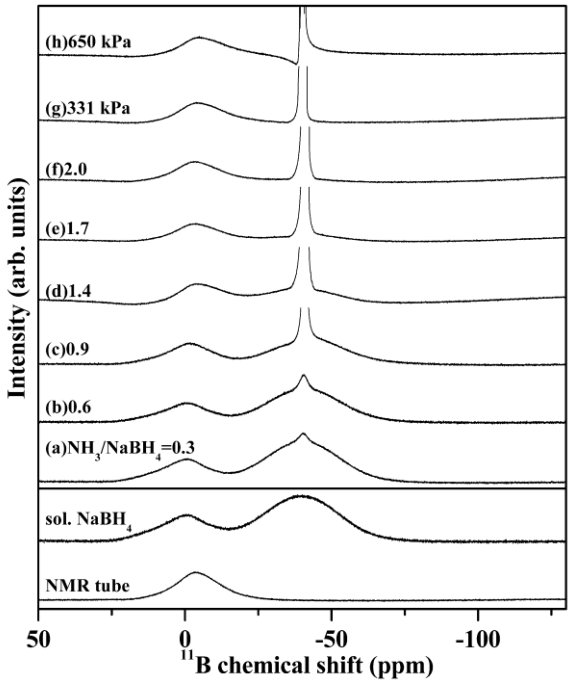

Figure 4.1.3 Some operand ^{11}B NMR results from Figure 4.1.2. Scale is normalized by the peak intensity of NMR tube (background).

In this figure, several data were chosen as representatives from Figure 4.1.2 ii and iii. The broad signal of solid $NaBH_4$ is appeared around -42.4 ppm. This broadening of the signal is caused by the limitation of molecular motion in solid states due to interactions such as dipolar and quadrupole interactions. At the lower pressure than the plateau pressure (Figure 4.1.2.i), the signals are not totally changed from the signal of solid $NaBH_4$, indicating that the reaction

between $NaBH_4$ and NH_3 did not proceed as the result of PCI measurement. At the plateau, a total of 2 mol NH_3 could be absorbed in $NaBH_4$ to form $Na(NH_3)_2BH_4$. With the increase in the amount of absorbed NH_3, the signal intensity related to the solid $NaBH_4$ is decreased with the appearance of a new sharp signal at -40.4 ppm, which is grown gradually. These phenomena are caused by the disappearance of the specific interactions of solids, in other words, the chemical states are averaged by the fast motion of molecules. Figure 4.1.4 shows the enlarged profile of Figure 4.1.2.ii-(e).

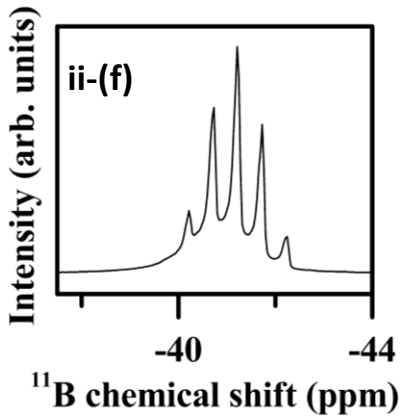

Figure 4.1.4 The enlarged profile of Figure 4.1.2.ii-(f)

The sharp signal is split into 5 peaks due to the spin-spin interactions in the B-H bonds[3]. In the previous reports, the peak splitting in solid state borohydride could not be observed by solid state ^{11}B NMR measurements at room temperature even by using magic angle spinning[4]. It can be suggested that the $Na(NH_3)_2BH_4$ phase generated in the plateau region is in liquid state. Namely, solid $NaBH_4$ and liquid $Na(NH_3)_2BH_4$ coexist at the plateau pressure. Actually, when the reaction of NH_3 absorption was performed in a glass vessel, the two phases separately exist at the plateau pressure as shown in the Figure 4.1.5. At the higher pressure than the plateau pressure, the phase is totally changed to

liquid as evidenced from the presence of the sharp signal only. Moreover, the peaks are slightly shifted to lower magnetic field with the increase in the NH_3 concentration. This phenomenon generally suggests that the electron density at B atom in the BH_4 anion is decreased. As one of the reasons to explain the above shift, it is suggested that the polarization of BH bonds is enhanced by the increase in the distance between the Na cation and the BH_4 anion.

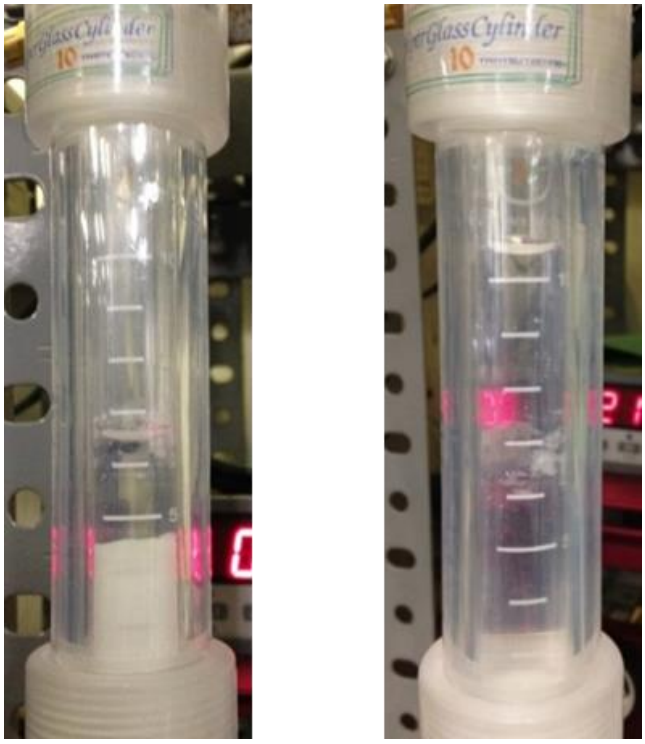

Figure 4.1.5 The images of $NaBH_4$ under the plateau pressure (left) and the higher pressure than the plateau pressure (right)

4.1.3 FT-IR measurements under NH_3 pressure

Figure 4.1.6 shows the FT-IR results of $NaBH_4$ under vacuum, 90, and 105 kPa of NH_3 pressure. The result without $NaBH_4$ under vacuum is also

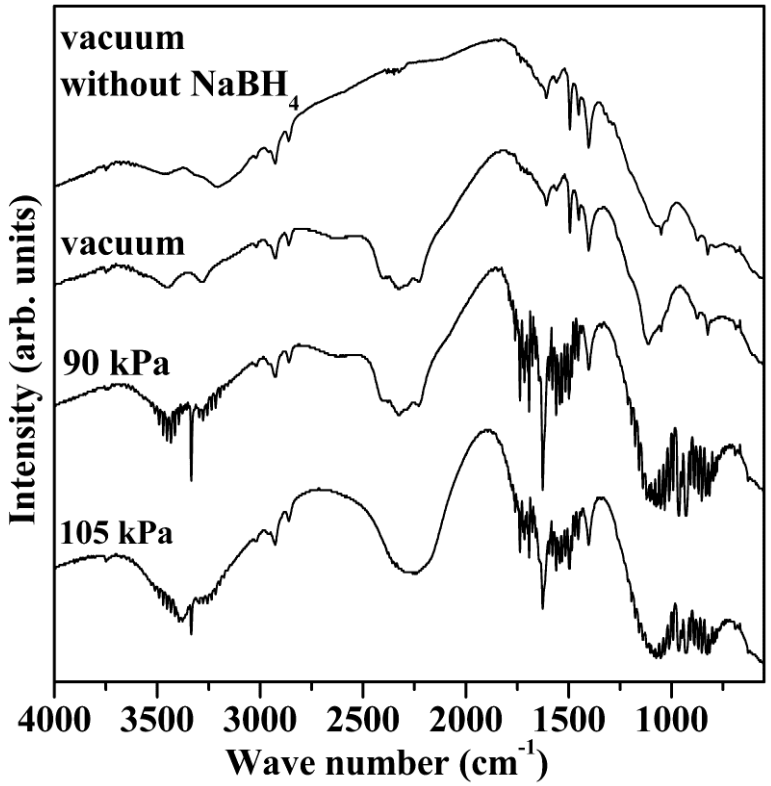

Figure 4.1.6 FT-IR results for background without $NaBH_4$, and for $NaBH_4$ under vacuum, 90 kPa, and 105 kPa of NH_3

shown as blank. Here, $NaBH_4$ doesn't absorb NH_3 under vacuum and 90 kPa, whereas liquid $Na(NH_3)_2BH_4$ phase is formed under 105 kPa of NH_3. In the $NaBH_4$-NH_3 system, N-H bond in NH_3 and B-H bond in $NaBH_4$ absorb infrared rays. Firstly, the absorption peaks related to N-H bonds are discussed. From the result of $NaBH_4$ under 90 kPa, many sharp signals were observed in the region around 500-1250, 1400-1800, and 3200-3750 cm^{-1} in addition to the result of $NaBH_4$ under vacuum. Since these series of peaks are characteristic signals for

gas phase, and $NaBH_4$ doesn't absorb NH_3 in this pressure, these signals are assigned to NH_3 gas in atmosphere. Furthermore, in the measurement under 105 kPa, a new peak was observed around 3400 cm^{-1}. This peak should be derived from NH_3 absorbed in $NaBH_4$. However, it is difficult to discuss the details because the peaks of gaseous NH_3 are essentially overlapped in the operando measurements. Therefore, the absorption peaks related to the B-H bonds are mainly discussed. The several peaks derived from the B-H bonds of solid $NaBH_4$ are observed in the wide range from 2100 to 2500 cm^{-1} under vacuum and 90 kPa[5, 6]. These peaks correspond to the symmetric and asymmetric stretching modes of B-H bonds of solid $NaBH_4$. In addition, on the basis of structural analysis by neutron diffraction, it has been reported that $NaBD_4$ contains two different B-D bonds with different bond lengths[7, 8]. The observed broad peak is formed by the B-H bonds with the various chemical states. On the other hand, the single peak related to B-H stretching is appeared at 2246 cm^{-1} for the sample under 105 kPa of NH_3, suggesting that the B-H bonds in the solid phase of $NaBH_4$ are averaged by liquefaction. These results are consistent with the results of ^{11}B NMR. Furthermore, the absorption peaks are shifted to low frequency after the NH_3 absorption. Here, it is known that, in alkali borohydrides and amides, the FT-IR peaks derived from B-H bonds or N-H bonds shift to low frequency with the decrease in the ionization energy of alkali metal species[9, 10]. Therefore, it can be considered that the peak shift in the $NaBH_4$-NH_3 system is caused by the decrease in ionization energy of Na cation due to the coordination of NH_3 to Na cation. As another possibility, the peak may also shift by the interaction between positively charged hydrogen in $NaBH_4$ and the negatively charged hydrogen in NH_3, which is called dihydrogen bond[11].

Actually, $NaBH_4 \cdot 2H_2O$ is known to have a dihydrogen bond formed between H in $NaBH_4$ and H in H_2O according to the analysis of crystal structure and infrared spectroscopy[5].

4.1.4 Operando ^{1}H NMR measurements under NH_3 pressure

Operando ^{1}H NMR measurements under various NH_3 pressure were carried out to investigate the chemical state of NH_3 and $NaBH_4$ solution, and the results are shown in Figure 4.1.7.i (lower pressure than plateau), ii (plateau), iii (higher pressure than plateau). The profile of pure liquid NH_3 without $NaBH_4$, solid $NaBH_4$, and sample tube are also shown as reference. The ^{1}H signals from the sample tube and solid $NaBH_4$ are hardly observed because these materials are solid and the interactions such as dipolar and quadrupole interactions are large.

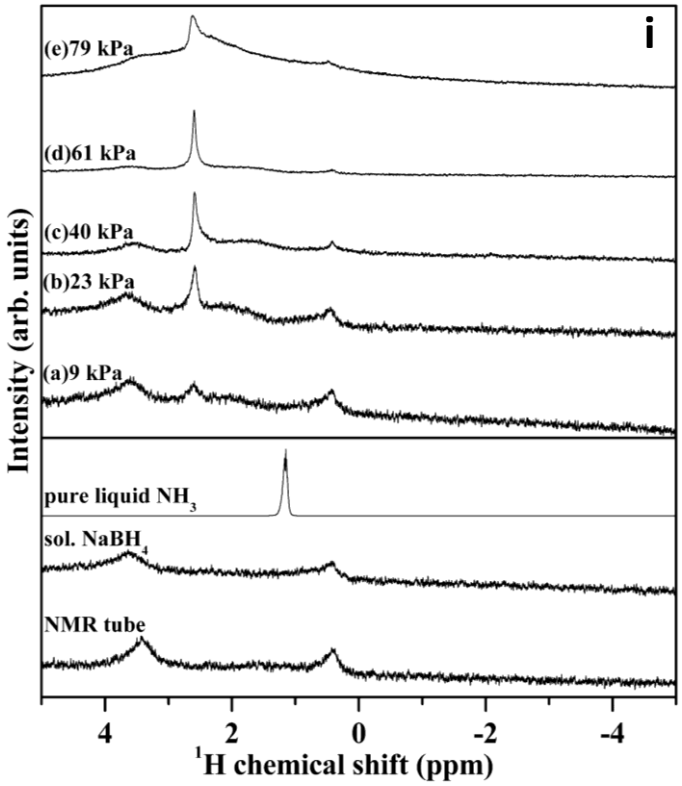

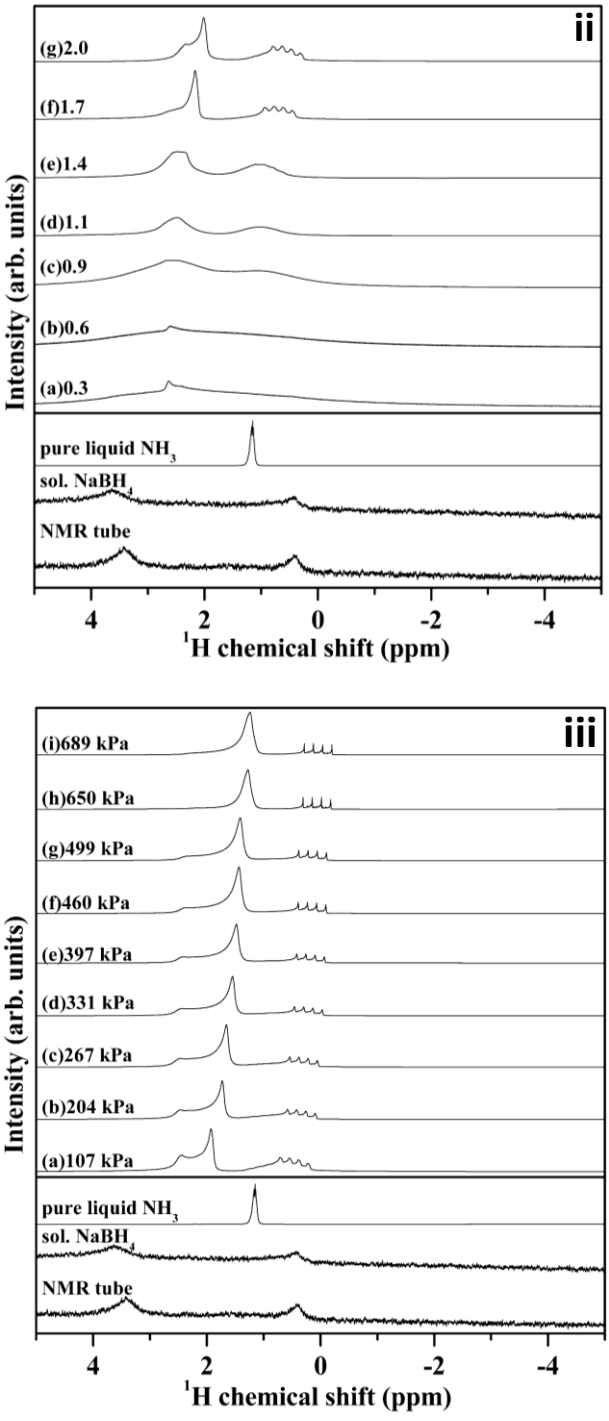

Figure 4.1.7 Operand ^{1}H NMR results for $NaBH_4$ (i) under the plateau pressure (ii) at the plateau region (iii) at the higher pressure than the plateau pressure

At the lower pressure than the plateau pressure, the signal related to gas NH_3 is appeared at 2.6 ppm and the intensity is gradually increased with the increase in the pressure of gas NH_3 compared with the peak intensity of NMR tube. In the result of 4.1.7-(e), the broad signal is observed around 0 to 4 ppm. It is considered that NH_3 gas is adsorbed on $NaBH_4$ or NMR tube. At the plateau pressure, it can be gradually and clearly observed the signal as the NH_3 absorption reaction proceeds and the liquid $Na(NH_3)_2BH_4$ is generated. With respect to the chemical shift in ^1H NMR, the signals of NH_3 and $NaBH_4$ are shifted to higher magnetic field with the increase in the absorbed NH_3, although the only ratio of solid $NaBH_4$ and liquid $Na(NH_3)_2BH_4$ is changed under the plateau pressure. It indicates that the local environment of H atoms is slightly changed possibly because solid $NaBH_4$ affects liquid $Na(NH_3)_2BH_4$, however, the detail is not understood yet. These signals are explained in detail as following sentences related to the Figure 4.1.7.iii. In the Figure 4.1.7.iii, a series of 4 signals with high intensity and 7 signals with low intensity are observed in the range from -0.2 to 0.3 ppm, as shown in Figure 4.1.8.

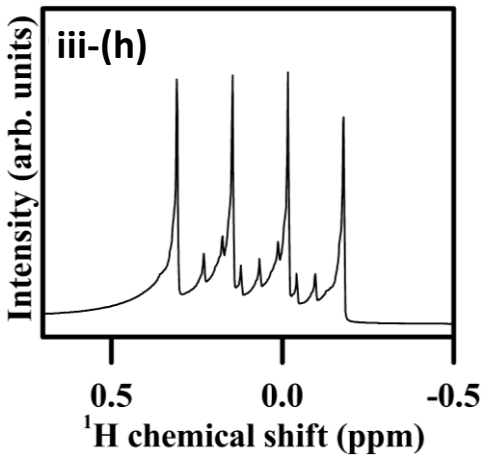

Figure 4.1.8 The enlarged profile of Figure 4.1.7.iii-(h)

Actually, $NaBH_4$ is composed of Na cation and BH_4 anion, and all the ^1H nuclei in the BH_4 anion are equivalent in the liquid state. Here, the nuclear spins of ^{11}B and ^{10}B are 3/2, 1/2, -1/2, -3/2 and 3, 2, 1, 0, -1, -2, -3, respectively, and the natural abundance ratio of them is 80:20. Therefore, signals originated in the ^1H nuclei in $NaBH_4$ split into 4 and 7 peaks corresponding to the spins of ^{11}B and ^{10}B, respectively. The difference in the intensities is caused by the abundance ratio. The ^1H NMR signals corresponding to $NaBH_4$ were observed under the NH_3 atmosphere, although the signal is not observed for the solid $NaBH_4$, suggesting that $NaBH_4$ is liquefied. The large signal around 1 – 1.5 ppm is assigned to liquid state NH_3. The shoulder peaks are thought to be originated from the different states of NH_3, i.e. strongly and weakly coordinated NH_3 to $NaBH_4$, although the details of origin are not understood completely yet. The shoulder peak actually disappeared with the increase in the NH_3 concentration. When it is considered in the same way as spin coupling in BH bonds, the ^1H signal related to NH_3 should be split into 3 peaks because the nuclear spins of ^{14}N is 1, 0, -1. Actually, the peak is split to 3 peaks for the pure liquid NH_3 as shown in Figure 4.1.9.

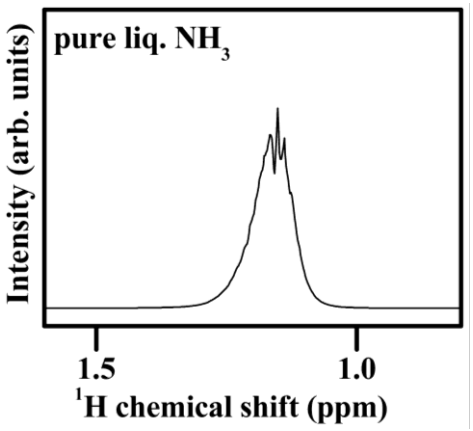

Figure 4.1.9 The enlarged profile of pure liquid NH_3

However, the peak splitting is not found in the $NaBH_4$-NH_3 system. Ogg et al. reported the similar phenomena in the $NaNH_2$-NH_3 system[12-14]. They added $NaNH_2$ into liquid NH_3 and carried out ^1H NMR measurements. In that case, the number of peaks of ^1H NMR signal is 1 due to the influence of $NaNH_2$. At the higher pressure than the plateau pressure, the signals of NH_3 and $NaBH_4$ are also shifted, and the similar phenomenon was confirmed in the case of ethanol-chloroform system. Ethanol can be written by the chemical formula of CH_3CH_2OH, and it was known that the hydrogen bonds are formed between OH groups. When chloroform, which is written by $CHCl_3$ and known as nonpolar solvent, was gradually added to ethanol, the signal of the OH groups shifted to the higher magnetic field because the hydrogen bonds between ethanol molecules are disturbed by chloroform[15]. From this perspective, the hydrogen bonds between NH_3 molecules in the $NaBH_4$-NH_3 system are considered as the reason for environmental change of NH_3 because it is reported that NH_3 molecules also form hydrogen bonds[16]. The peak shift of $NaBH_4$ to higher magnetic field with the increase in the NH_3 concentration corresponds to the increase of the electron density of H in BH_4 anion. Here, the electron density of B in BH_4 anion is decreased as discussed above. Namely, the electron density of H in BH_4 anion is increased to keep the electrical balance. This peak shift is possibly occurred by the polarization of the BH bonds and longer distance between the Na cation and BH_4 anion due to the increase in the NH_3 concentration.

4.1.5 Operando ^{11}B NMR measurements under NH_3 pressure

The PCI curve is analyzed in terms of ideal and regular solutions. Here, the PCI measurement was performed at 0 °C to analyze up to the higher NH_3 pressure than the plateau pressure (see Figure 4.1.10).

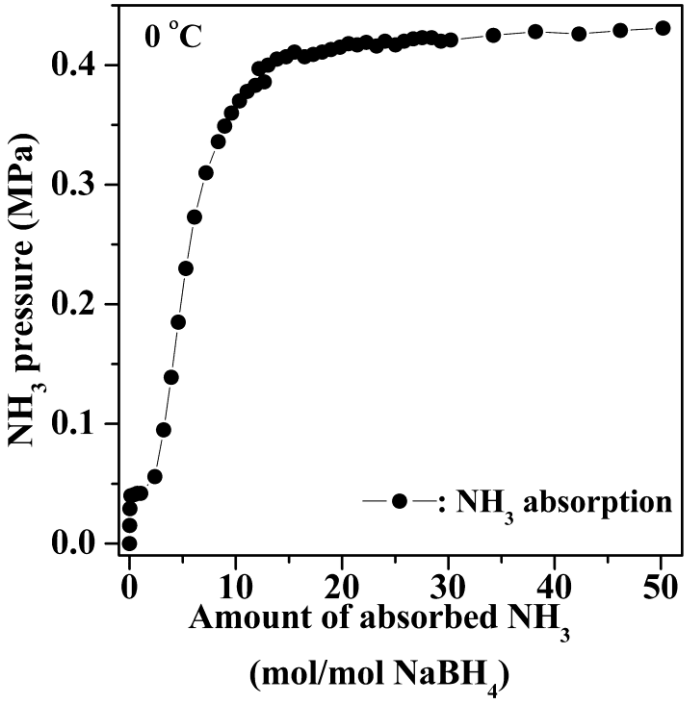

Figure 4.1.10 PCI measurement for NH_3 absorption of $NaBH_4$ at 0 °C

In the ideal solution, the heat generated by mixing the two materials in liquid state is negligible. On the other hand, in the regular solution, the heat generated due to the mixing should be considered. Here, in solution theory, the mixing between liquids is considered. In the $NaBH_4$-NH_3 system, since two phases of solid $NaBH_4$ and liquid $Na(NH_3)_2BH_4$ coexist at the plateau pressure, it was considered as a mixture of liquid $Na(NH_3)_2BH_4$ and liquid NH_3 in a pressure region higher than the plateau pressure. In $Na(NH_3)_2BH_4$-NH_3 solution, the

chemical potential of the liquid and gas phase is denoted as μ_l and μ_g, respectively, and defined as follows,

$$\mu_l = \mu_l^0 + \Delta H + RT\ln X_{NH3}, \quad (4.1.1)$$

$$\mu_g = \mu_g^0 + RT\ln(P/P_0). \quad (4.1.2)$$

P is the NH_3 vapor pressure. The chemical potential of the liquid and gas phase for pure NH_3 is μ_l^0 and μ_g^0, respectively. P_0 is the NH_3 vapor pressure at standard state. T is the reaction temperature, ΔH is enthalpy change by mixing, R is the gas constant, and X_{NH3} is defined by the following equation,

$$X_{NH3}=n_{NH3}/(n_{NH3}+n_{Na(NH3)2BH4}+\alpha n_{Na(NH3)2BH4}). \quad (4.1.3)$$

Here, n_{NH3} and $n_{Na(NH3)2BH4}$ are the molar amount of NH_3 and $Na(NH_3)_2BH_4$, respectively. α is ionization of $Na(NH_3)_2BH_4$. Therefore, $X_{NH3,\ \alpha=0}$ and $X_{NH3,\ \alpha=1}$ are expressed by the following equation,

$$X_{NH3,\ \alpha=0}= n_{NH3}/(n_{NH3}+n_{Na(NH3)2BH4})=x_{NH3}, \quad (4.1.4)$$

$$X_{NH3,\ \alpha=1}=n_{NH3}/(n_{NH3}+2n_{Na(NH3)2BH4})= x_{NH3}/(2- x_{NH3}). \quad (4.1.5)$$

The relative pressure P/P_0 at equilibrium condition ($\mu_g^0=\mu_l^0$, $\mu_g=\mu_l$) is shown as follow,

$$P/P_0=\exp(\Delta H/RT+\ln X_{NH3}). \quad (4.1.6)$$

Here, the relative pressure P normalized by the plateau pressure is replaced by the relative pressure P/P_0, and the P, in the case of ideal and regular solution of degree of ionization α=0 or 1, is expressed as follows[17],

ideal: $P = x_{NH3}$ ($\alpha = 0$), (4.1.7)

$= x_{NH3}/(2-x_{NH3})$ ($\alpha = 1$), (4.1.8)

regular: $P = \exp(\Delta H/RT+\ln x_{NH3})$ ($\alpha = 0$), (4.1.9)

$= \exp(\Delta H/RT+\ln(x_{NH3}/(2-x_{NH3}))$ ($\alpha = 1$). (4.1.10)

The x_{NH3}-P curves for $NaBH_4$-NH_3 system of ideal and regular solution are

shown in Figure 4.1.11. The experimental data are matched with the curve of the regular solution (α=1) in the region from x_{NH3}=0.0 to 0.7 in the case of ΔH=−6 kJ/mol. On the other hand, the curve at high NH_3 concentration region from x_{NH3}=0.9 to 1.0 are well consistent with that of the ideal solution (α=0). From the above, the regular solution (α=1) is changed to the ideal solution (α=0) with the increase in x_{NH3}.

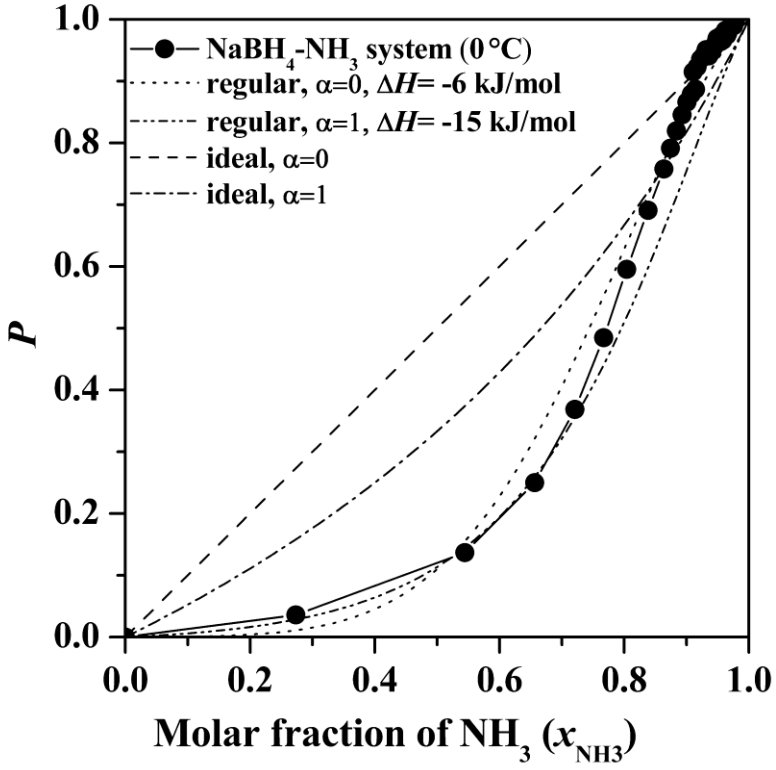

Figure 4.1.11 NH_3 absorption curve of $NaBH_4$ and results of analyses by assuming ideal and regular solution at 0 °C. The heat of mixing is -6 and -15 kJ/mol for regular solution of α=0 and 1 system

4.2 Catalytic effects of NH_3 absorbing materials on H_2 generation of NH_3-LiH system

4.2.1 The additive effects of Ti, TiH_2, LiCl

Figure 4.2.1 shows the XRD patterns of LiH with Ti, TiH_2, and LiCl. The result of the as-milled LiH without additives is also shown as reference.[18]

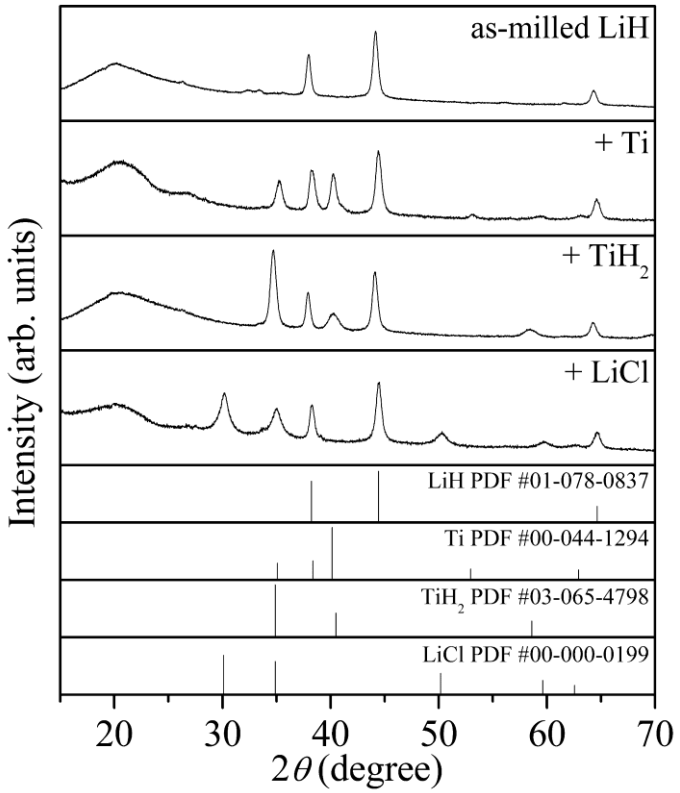

Figure 4.2.1 XRD patterns of the LiH with no additive, Ti, TiH_2, and LiCl after the ball-milling

In addition, the XRD patterns of LiH (PDF#01-078-0837), Ti (PDF#00-044-1294), TiH_2 (PDF#03-065-4798), and LiCl (PDF#00-000-0199) are referred from databases in PDXL. Here, the broad peaks observed around 20 and 25° are caused by a grease as glue to fix the powder sample and the polyimide sheet

to avoid oxidation of the samples. In general, the ball-milling decreases crystalline size and induces structural disorder, such as defects, resulting in characteristic diffraction peaks with low intensity and broad shapes[19]. Here, the crystallite size and the lattice strain can be estimated by the Williamson–Hall equation[20],

$$\beta\cos\theta = 2\eta\sin\theta + \lambda/\varepsilon \quad (4.2.1)$$

where β is the half-value width, θ the Bragg angle, λ is the X-ray wavelength, η the crystallite size and ε the lattice strain. In this system, θ and λ is the common value for all the samples. Furthermore, after the ball-milling, the intensity and shape of the diffraction peaks were similar, where the intensity was relatively compared with a background due to the polyimide sheet and the grease. Thus, the crystalline size and the degree of crystal disorder of LiH was almost the same for all the samples. Therefore, it was expected that the contribution of the ball-milling for the reaction yield is not changed largely for all the LiH samples. For the LiH with additives, the broad peaks corresponding to Ti, TiH_2, and LiCl were also observed without generating any other products, suggesting that the additives were stable in the ball-milling process.

The reaction between each LiH sample with the additive and 0.45 MPa of NH_3 was carried out, and the XRD results after the reaction for 24 h at room temperature are shown in Figure 4.2.2. It was clearly found that $LiNH_2$ was formed in all the samples after the reaction, indicating that the expected H_2 generation reaction proceeded, although a part of LiH as the reactant remained. The small peaks of Ti and TiH_2 were confirmed, while it was difficult to identify LiCl because the diffraction peaks were overlapped to those of $LiNH_2$ or possibly changed to other phases with low crystallinity.

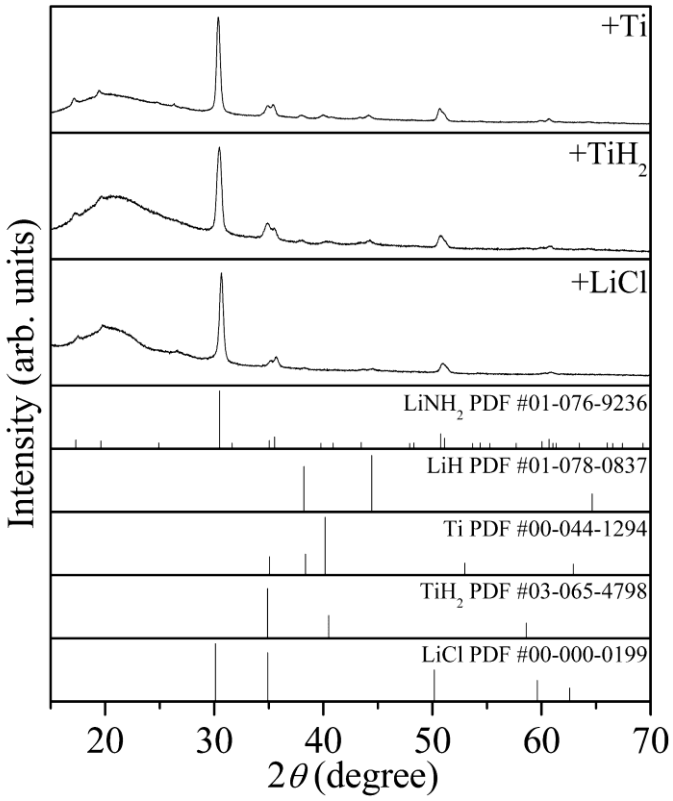

Figure 4.2.2 XRD patterns of the product after the reaction between LiH with additives and NH_3 for 24 h

The reaction yield is estimated by the weight gain of the LiH samples after the reaction for 1, 12, and 24 h at room temperature, and the results are plotted as a function of time in Figure 4.2.3. The reaction rates of as-milled LiH and LiH with $TiCl_3$ are also shown to be compared.[18] Here, the standard deviation ±3% is representatively shown in the data of the LiH with $TiCl_3$ because some data points are overlapped. To calibrate the experimental data and to estimate essential reaction yields, the weight change by the NH_3 absorption into LiCl itself under 0.45 MPa was also measured by the same procedure as the H_2 generation reaction. As a result, it was confirmed that about 1.0 mol of NH_3 remained into 1.0 mol of LiCl after the vacuum process.

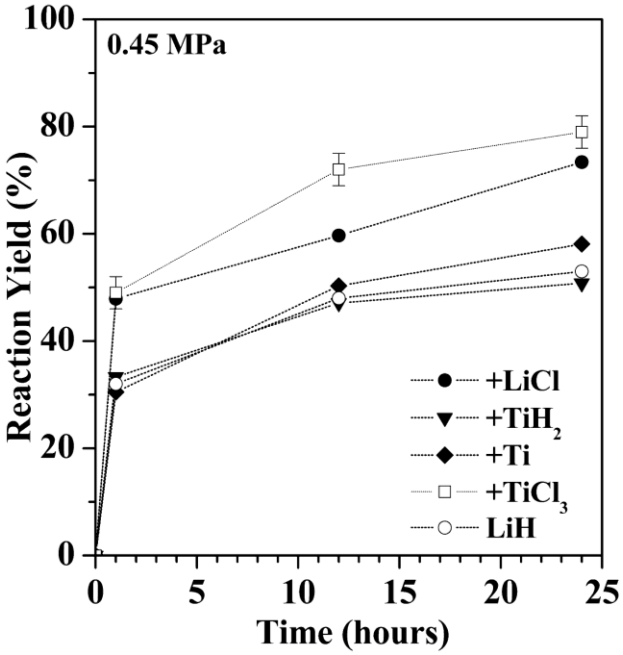

Figure 4.2.3 Reaction yield of the LiH with no additive, $TiCl_3$, Ti, TiH_2, and LiCl as a function of time under 0.45 MPa of NH_3 pressure

On the basis of the obtained data for the weight change of LiCl, the reaction yield for LiH with LiCl and $TiCl_3$ was calibrated, where the LiCl formation during the ball-milling was clarified in the case of $TiCl_3$ additive as described above[18]. The reaction yields of the LiH with Ti and TiH_2 for all the measurement times were almost the same as those of the LiH without additives, suggesting that no additive effects were shown. On the other hand, the LiCl-dispersing LiH revealed about 50 and 70% of reaction yield after 1 and 24 h, respectively. These values are close to the results of the LiH with $TiCl_3$. It is suggested that LiCl has the significant catalytic effect. In gas−solid reactions, conventional metal catalysts such as Ni, Pd, and Pt with d- and f-electrons generally affect dissociation of gaseous molecule by electronic interaction.[21-23] In this manner, it is expected that Ti with d-electron would improve the kinetic properties.[24, 25]

However, it is noteworthy that LiCl, which is a simple ionic crystal with closed-shell electron structure, revealed the significant catalytic effect, indicating that the catalytic mechanism of LiCl on the reaction between NH_3 and LiH is quite different from the conventional ones.

4.2.2 The NH_3 absorbing properties of LiCl, $LiBH_4$, $NaBH_4$[1]

In our laboratory, it has been investigated that various halides and borohydrides absorb molecular NH_3 and form an ammine complex, which is a complex with NH_3 as a ligand[1, 2, 26-28]. LiCl, which shows catalytic effect for the NH_3-LiH system in the previous section, possess the NH_3 absorbing properties, and the reaction is expressed by the following equation[1, 29],

$$LiCl + xNH_3 \leftrightarrow Li(NH_3)_xCl. \quad (4.2.2)$$

Figure 4.2.4 shows a PCI curve of LiCl.[1]

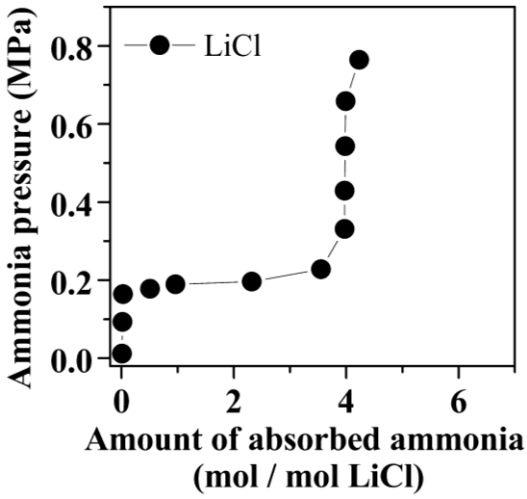

Figure 4.2.4 The NH_3 absorption property of LiCl

With introducing NH_3 to sample cell with LiCl, the NH_3 pressure only increase at the less than plateau pressure because the reaction between LiCl and NH_3 did not proceed. And then, the plateau appeared at 0.178 MPa, indicating that the NH_3 absorbing reaction occurred. 1.0 mol of LiCl absorb 4.0 mol of NH_3 from the result of PCI measurement. When NH_3 was further introduced, the pressure only increased as the case of less than plateau pressure, thus, the reaction does

not proceed in the higher pressure than the plateau pressure. The experimental pressure for NH_3-LiH system is 0.45 MPa and $Li(NH_3)_4Cl$ is formed in this pressure. From the above, we focused on the NH_3 absorbing properties of LiCl to understand mechanism of the catalytic effect for the NH_3-LiH system. $LiBH_4$ and $NaBH_4$ were chosen as other additives to investigate the correlation between the NH_3 absorbing properties and the catalytic effects. Figure 4.2.5 shows the result of PCI measurements for $LiBH_4$ and $NaBH_4$.[1] $LiBH_4$ and $NaBH_4$ absorb about 3.5 and 5.2 mol of NH_3 under 0.45 MPa, respectively. In addition, these materials are chemically stable, in other words, the materials are expected not to be changed by mechanical energy applied during the ball-milling to be dispersed into LiH.

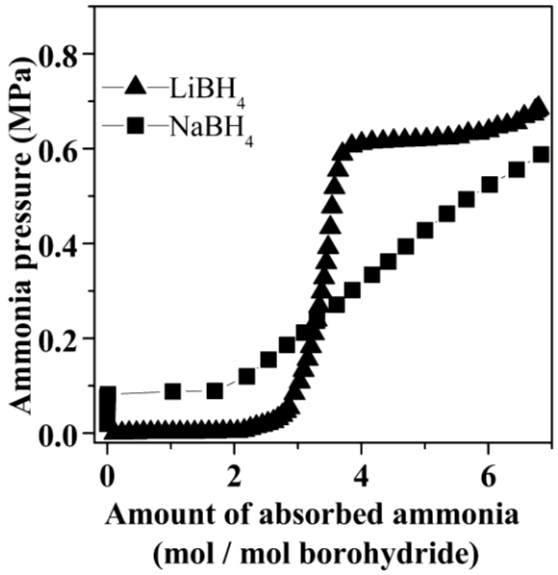

Figure 4.2.5 The NH_3 absorption property of $LiBH_4$ and $NaBH_4$

4.2.3 The additive effect of NH_3 absorbing materials

The XRD patterns of LiH with $LiBH_4$ and $NaBH_4$ after the ball-milling are shown in Figure 4.2.6.

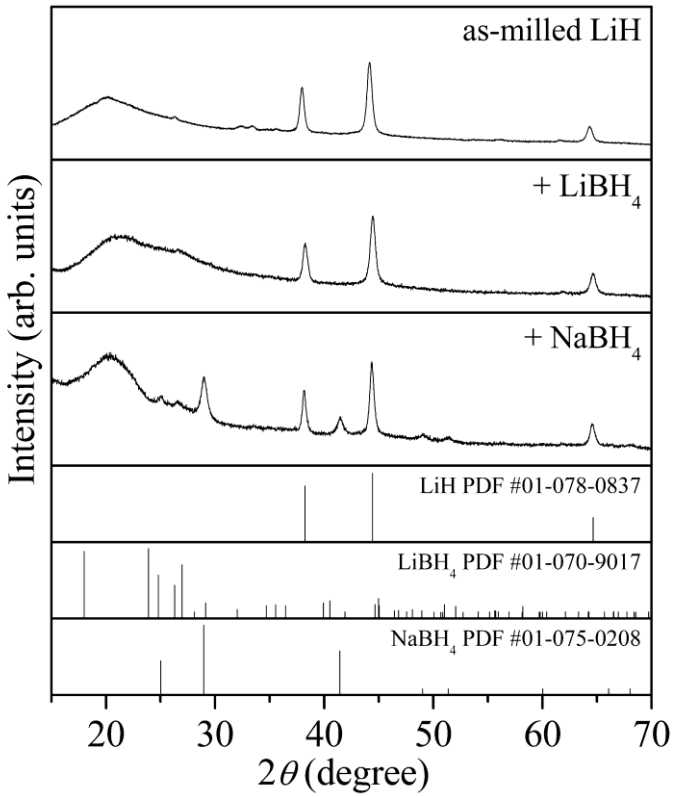

Figure 4.2.6 XRD patterns of the LiH with $LiBH_4$ or $NaBH_4$ after the ball-milling

From the diffraction intensity and peak shape of LiH, it was found that the milling effects have no obvious difference between LiH without and with the additives as well as the above Ti series. Thus, the structural properties would not affect the reactivity with NH_3. The diffraction peaks corresponding to $NaBH_4$ were observed, suggesting that it is stable and not changed during the ball-milling. In the case of LiH with $LiBH_4$, no other peaks except for LiH appeared. Since $LiBH_4$ is thermodynamically stable and $LiBH_4$ is not changed

by the exchange of cation as the case of $TiCl_3$ due to Li cation in both of the starting materials, it is considered that $LiBH_4$ forms a nano or amorphous state.

The reaction between LiH with borohydride additives and 0.45 MPa of NH_3 was carried out, and the XRD results after the reaction for 24 h at room temperature are shown in Figure 4.2.7.

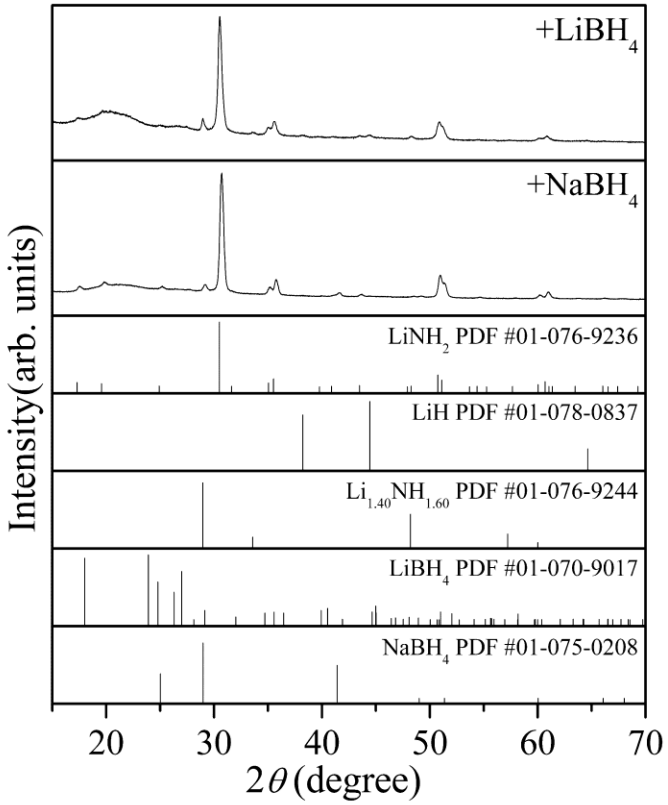

Figure 4.2.7 XRD patterns of the product after the reaction between LiH with borohydride additives and NH_3 for 24 h

The $LiNH_2$ formation was clearly observed for both samples. Among them, LiH completely disappeared in the case of $NaBH_4$ additive even though the small peaks of LiH was found in the XRD patterns of LiH with LiCl (Figure 4.2.2) and $LiBH_4$. Therefore, it was expected that LiH with $NaBH_4$ shows higher

reactivity than others. Here, in the XRD pattern of LiH with $LiBH_4$, small extra peaks were also found around 28, 33, and 48°, which are possibly assigned to $Li_{1.40}NH_{1.60}$ (01−076−9244). As another possibility, it is thought that the diffraction peaks originated in the ammine complex of $LiBH_4$ are observed. Because it was indicated that approximately 2.0 mol of NH_3 remained in 1.0 mol of $LiBH_4$ after the NH_3 absorption and desorption test performed to calibrate the weight gain like the case of LiCl.

Figure 4.2.8 shows the reaction yields of the LiH with the NH_3 absorbing materials for 1, 12, and 24 h at room temperature.

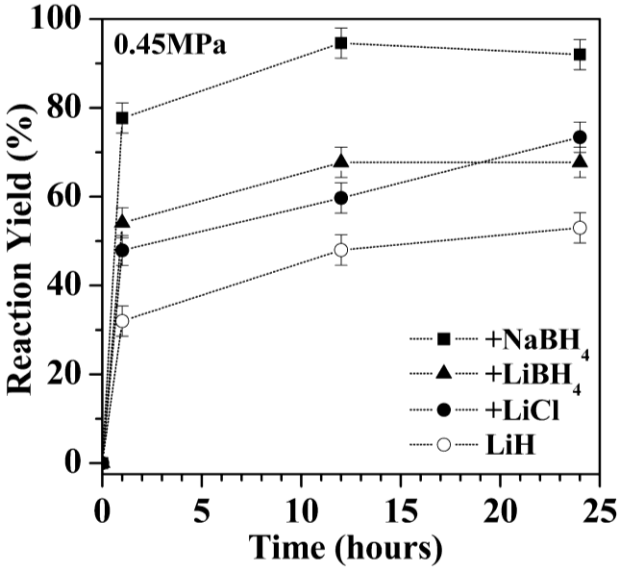

Figure 4.2.8 Reaction yield of the LiH with no additive, $LiBH_4$, and $NaBH_4$ as a function of time under 0.45 MPa of NH_3 pressure

The reaction yields of the ball-milled LiH is also shown as reference. The calibrated values related to the residual NH_3 in the NH_3 absorbing materials after the reaction are plotted for LiH with LiCl and $LiBH_4$. In the case of $NaBH_4$, it was clarified that all NH_3 was released during the experimental procedure[1]. In

addition, the reaction yield after 24 h, the amount of the absorbed NH_3 based on PCI results, and the plateau pressure of each additive are listed and compared in Table 4.2.1. LiH without additives showed about 50% of reaction yield for 24 h. The reaction behaviors of LiH with LiCl and $LiBH_4$ are quite similar. The reaction rate for both samples was faster than that of LiH, resulting in about 50% of reaction yield for only 1 h. As shown in Table 4.2.1, 4.0 and 3.5 mol of NH_3 is absorbed under 0.45 MPa for LiCl and $LiBH_4$, respectively. It is thus indicated that the catalysis is related to the NH_3 absorption properties. In fact, $NaBH_4$, which can absorb 5.2 mol of NH_3, revealed the drastic catalytic effect. As a result, the reaction yield was about 80% for only 1 h and reached to more than 90% for 12 h.

Table 4.2.1 List of the experimental pressure *P*, the equilibrium plateau pressure for the NH_3 absorption P_{eq}, the absorbed amount of NH_3, and the yield of the reaction for 24 h

P (MPa)	sample	P_{eq}(MPa)	Absorbed NH_3 (mol/mol additive)	Reaction yield (%)
0.45	LiH	-	-	53
	LiCl	0.178	4.0	73
	$LiBH_4$	<0.001	3.5	68
	$NaBH_4$	0.093	5.2	92
0.10	LiH	-	-	30
	LiCl	0.178	0.0	34
	$LiBH_4$	<0.001	3.0	70
	$NaBH_4$	0.093	2.0	-

To understand the correlation between the catalytic effect for the H_2 generation and the NH_3 absorption into catalysts more clearly, the reaction for

LiH with LiCl and $LiBH_4$ was carried out under 0.10 MPa of NH_3 for 1, 12, and 24 h. It was noted that the catalysis of LiCl was clearly lost, and then the curve of reaction yield was the same as that of LiH without additives, as shown in Figure 4.2.9.

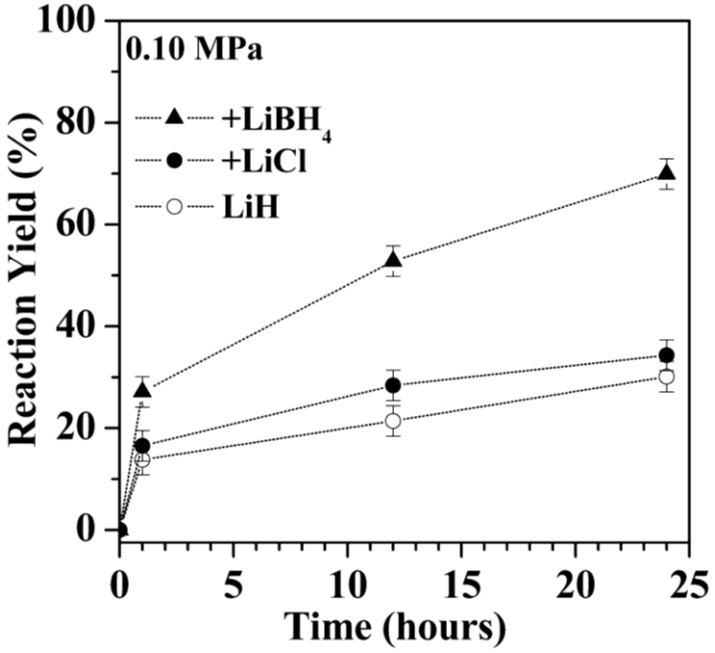

Figure 4.2.9 Reaction yield of the LiH with no additive, $LiBH_4$, and $NaBH_4$ as a function of time under 0.10 MPa of NH_3 pressure

On the other hand, the high reactivity of LiH with $LiBH_4$ was preserved, and the reaction yield for 24 h is almost the same as that obtained under 0.45 MPa. The different behavior is caused by the NH_3 absorption properties of them. As shown in Table 1, the equilibrium plateau pressure for the NH_3 absorption of LiCl and $LiBH_4$ is 0.178 and less than 0.001 MPa, respectively. Namely, NH_3 is not absorbed in LiCl at 0.10 MPa, while $LiBH_4$ still absorb 3.0 mol of NH_3 at the same pressure. Therefore, it is concluded that the catalysis is strongly related to the NH_3 absorption properties of the catalysts.

4.2.4 The catalytic mechanism of the NH_3 absorbing materials for the NH_3-LiH system

From the above results, the catalytic mechanism of the NH_3 absorbing materials for the NH_3-LiH system is discussed. Figure 4.2.10 shows models of the reaction for LiH with and without catalysts.

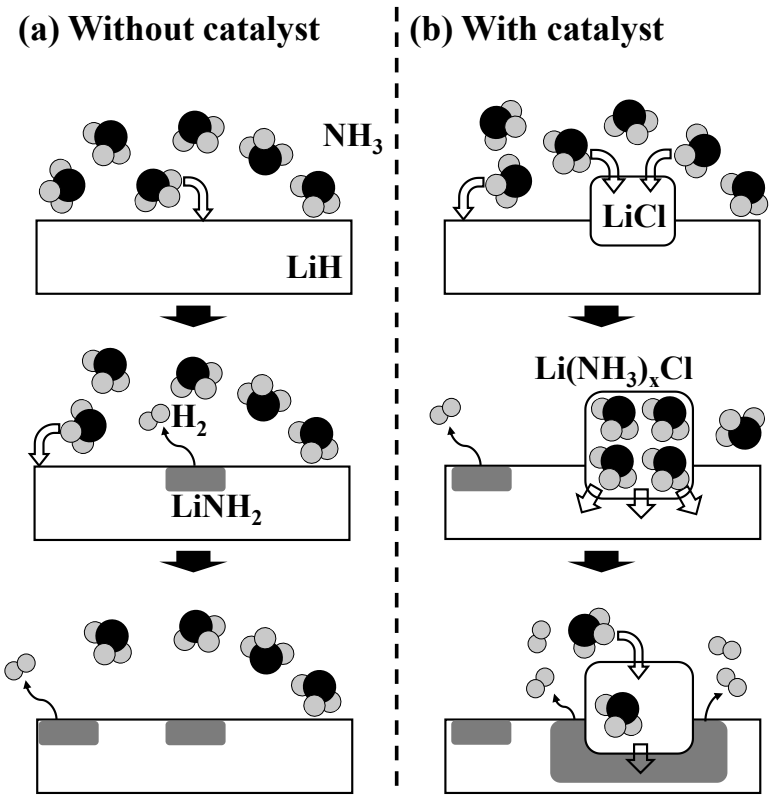

Figure 4.2.10 Schematic image of reaction model for (a) random collision process for the LiH without additives and (b) catalytic processes for the LiH with LiCl

For the LiH without catalysts, gaseous NH_3 randomly collides a LiH surface in a manner of general gas−solid reaction, as shown in Figure 4.2.10-(a). In the case of LiH with catalysts such as LiCl and borohydrides, the highly condensed state of NH_3 is generated into catalysts because NH_3 is absorbed as a molecular

state, as shown in Figure 4.2.10-(b), indicating that the frequency of collision between NH_3 and LiH is increased. The similar phenomena were reported by Matsumoto et al. for the NH_3 mediated model of the Li-N-H system, as described above[30]. Authors claimed that the catalyst increases frequency factor of the H_2 generation reaction, and then the catalyst plays a role of the NH_3 diffusion path. Thus, it is possible that the catalytic effects discussed in the literature and proposed in this work might be similar. In the reaction model shown in Figure 4.2.10-(b), the condensed NH_3 into catalysts should be transferred to LiH. In this case, a diffusivity of the absorbed NH_3 would be an important factor to realize immediate delivery of NH_3 molecules to the LiH phase. The entropy would be one of the factors to discuss the motion of NH_3 in the ammine complex. The thermodynamic properties of the reaction between $NaBH_4$ and NH_3 were evaluated by using PCI measurements at different temperatures and reported[1]. In this literature, the entropy change of ΔS^0 of the following reaction was estimated to be about −98 J/(mol K),

$$NaBH_4 + 2NH_3 \leftrightarrow Na(NH_3)_2BH_4 \quad (4.2.3)$$

Here, S^0 of gaseous NH_3 and $NaBH_4$ are 192 and 101 J/(mol K), respectively.[31] Therefore, S^0 of $Na(NH_3)_2BH_4$ is estimated to be 289 J/(mol K) by (-98*2+192*2+101). The entropy of $Na(NH_3)_2BH_4$ is very high compared with $NaBH_4$ itself, although it is expected that the absolute value of ΔS^0 is almost equal to S^0 of gaseous phase in a gas−solid reaction such as conventional metal and hydrogen systems. In addition to the above report, Sørby et al. reported that the ND_3 molecules in the hexa-ammine complex of $MgCl_2$, which is described as $Mg(ND_3)_6Cl_2$, possesses the highly correlated rotational and translational motions[26]. Thus, it can be speculated that the active motion of absorbed NH_3

molecules or both of the complex anion BH_4^- and NH_3 in the ammine complex realizes the high degree of freedom of $Na(NH_3)_2BH_4$. This high entropy state would induce the high diffusivity of NH_3, resulting in fast transfer of NH_3 to neighboring LiH. Furthermore, under 0.45 MPa, the large amount of NH_3 can be absorbed into $NaBH_4$, and then a liquid state of ammine complex is formed[1]. The melting phenomenon should further enhance the diffusivity of NH_3 and accelerate the reaction rate. In addition, the ammine complex phase should be relatively unstable compared with the $LiNH_2$ formation. If the NH_3 absorption state is stable, it is expected that the kinetic improvement based on the above mechanism will not be shown because the ammine complex phase is difficult to release NH_3 molecules. In fact, it was reported that the reactivity between $Mg(NH_3)_xCl_2$, which is typically stable ammine complex, and LiH was poor around room temperature, and a heat activation is necessary for the reaction to progress[32].

References

1. T. Aoki, T. Ichikawa, H. Miyaoka and Y. Kojima, *The Journal of Physical Chemistry C*, 2014, **118**, 18412-18416.
2. T. Zhang, H. Miyaoka, H. Miyaoka, T. Ichikawa and Y. Kojima, *ACS Applied Energy Materials*, 2018, **1**, 232-242.
3. J. Hannauer, U. B. Demirci, C. Geantet, J. M. Herrmann and P. Miele, *Physical Chemistry Chemical Physics*, 2011, **13**, 3809-3818.
4. M. H. W. Verkuijlen, P. Ngene, D. W. de Kort, C. Barré, A. Nale, E. R. H. van Eck, P. J. M. van Bentum, P. E. de Jongh and A. P. M. Kentgens, *The Journal of Physical Chemistry C*, 2012, **116**, 22169-22178.
5. Y. Filinchuk and H. Hagemann, *European Journal of Inorganic Chemistry*, 2008, **2008**, 3127-3133.
6. O. Zavorotynska, M. Corno, A. Damin, G. Spoto, P. Ugliengo and M. Baricco, *The Journal of Physical Chemistry C*, 2011, **115**, 18890-18900.
7. R. L. Davis and C. H. L. Kennard, *Journal of Solid State Chemistry*, 1985, **59**, 393-396.
8. P. Fischer and A. Züttel, *Materials Science Forum*, 2004, **443-444**, 287-290.
9. G. Renaudin, S. Gomes, H. Hagemann, L. Keller and K. Yvon, *Journal of Alloys and Compounds*, 2004, **375**, 98-106.
10. T. Takao, S. Tatsuya and O. Tamio, *Journal of Physics: Condensed Matter*, 2009, **21**, 185501.
11. R. Custelcean and J. E. Jackson, *Chemical Reviews*, 2001, **101**, 1963-1980.
12. R. A. Ogg, *The Journal of Chemical Physics*, 1954, **22**, 560-561.
13. R. A. Ogg and J. D. Ray, *The Journal of Chemical Physics*, 1957, **26**, 1515-1516.
14. R. A. Ogg, *Discussions of the Faraday Society*, 1954, **17**, 215-220.
15. T. D. Ferris, M. D. Zeidler and T. C. Farrar, *Molecular Physics*, 2000, **98**, 737-744.
16. W. L. Jorgensen and M. Ibrahim, *Journal of the American Chemical Society*, 1980, **102**, 3309-3315.
17. T. Hanai, *Kagakudojin, Kyoto*, 1978, 131-145.

18. H. Miyaoka, H. Fujii, H. Yamamoto, S. Hino, H. Nakanishi, T. Ichikawa and Y. Kojima, *International Journal of Hydrogen Energy*, 2012, **37**, 16025-16030.
19. N. Hanada, T. Ichikawa, S.-I. Orimo and H. Fujii, *Journal of Alloys and Compounds*, 2004, **366**, 269-273.
20. G. K. Williamson and W. H. Hall, *Acta Metallurgica*, 1953, **1**, 22-31.
21. M. Y. Song, *Journal of Materials Science*, 1995, **30**, 1343-1351.
22. N. Hanada, T. Ichikawa and H. Fujii, *The Journal of Physical Chemistry B*, 2005, **109**, 7188-7194.
23. S. Isobe, T. Ichikawa, J. I. Gottwald, E. Gomibuchi and H. Fujii, *Journal of Physics and Chemistry of Solids*, 2004, **65**, 535-539.
24. G. Liang, J. Huot, S. Boily, A. Van Neste and R. Schulz, *Journal of Alloys and Compounds*, 1999, **292**, 247-252.
25. K. Yamamoto, S. Tanioka, Y. Tsushio, T. Shimizu, T. Morishita, S. Orimo and H. Fujii, *Journal of Alloys and Compounds*, 1996, **243**, 144-150.
26. M. H. Sørby, O. M. Løvvik, M. Tsubota, T. Ichikawa, Y. Kojima and B. C. Hauback, *Physical Chemistry Chemical Physics*, 2011, **13**, 7644-7648.
27. T. Aoki, H. Miyaoka, H. Inokawa, T. Ichikawa and Y. Kojima, *The Journal of Physical Chemistry C*, 2015, **119**, 26296-26302.
28. H. Miyaoka, H. Miyaoka, T. Ichikawa, T. Ichikawa and Y. Kojima, *International Journal of Hydrogen Energy*, 2018, **43**, 14486-14492.
29. M. M. Szczęśniak, Z. Latajka, P. Piecuch, H. Ratajczak, W. J. Orville-Thomas and C. N. R. Rao, *Chemical Physics*, 1985, **94**, 55-63.
30. M. Matsumoto, T. Haga, Y. Kawai and Y. Kojima, *Journal of Alloys and Compounds*, 2007, **439**, 358-362.
31. NIST, *https://webbook.nist.gov/chemistry/*.
32. M. Tsubota, S. Hino, H. Fujii, C. Oomatsu, M. Yamana, T. Ichikawa and Y. Kojima, *International Journal of Hydrogen Energy*, 2010, **35**, 2058-2062.

5 Conclusion

In this thesis, we focused on sodium borohydride ($NaBH_4$) as an NH_3 absorbing material and catalysts. The NH_3 absorption properties have been analysed and discussed based on the results obtained by using operando spectroscopic analyses method. Furthermore, the catalysis for the hydrogen generation of the NH_3−LiH system were investigated to clarify the catalytic mechanism in this system.

The NH_3 absorption properties of $NaBH_4$ were analysed and discussed based on the results obtained by operando spectroscopic analyses under NH_3 atmosphere. It is clarified from the operando ^{11}B, ^{1}H NMR, and FT-IR that $Na(NH_3)_xBH_4$, which is formed by the NH_3 absorption of $NaBH_4$, is in the liquid state in all the region of the NH_3 concentration. For $NaBH_4$, it is suggested that the polarization between the BH bonds increases with the increase in the NH_3 concentration. In fact, ^{11}B and ^{1}H NMR signals originated in $NaBH_4$ are shifted to the opposite direction. For NH_3, the hydrogen bonds between the NH_3 inter-molecules in the $NaBH_4$−NH_3 system is found to be weaker than those in pure liquid NH_3. Through the analysis based on solution theory for $Na(NH_3)_xBH_4$, it is suggested that the liquid solution is changed from the regular solution (α=1) to the ideal solution (α=0) with the increase in the molar ratio of NH_3. In conclusion, for the NH_3 absorption of $NaBH_4$ with liquefaction, the N-H and B-H bonds interact each other and their chemical states change with the NH_3 concentration.

For the H_2 generation of the NH_3−lithium hydride (LiH) system, the NH_3 absorbing materials, which are lithium chloride (LiCl), lithium borohydride ($LiBH_4$), and $NaBH_4$, show significant catalytic effects. Among them, $NaBH_4$ was the most effective catalyst, and the reaction yield reached to more than 90% for 12 h. It is clarified that the catalysis was strongly related to the NH_3 absorption properties. In the NH_3 absorbed state, the condensation state of NH_3 is generated, and the NH_3 molecules could possess the high diffusivity, suggesting that the absorbed and condensed NH_3 is easily transferred into the neighboring LiH phase and reacts to generate H_2. Furthermore, the melting phenomenon of $NaBH_4$ by NH_3 absorption, which is clarified in our spectroscopic analyses, should further enhance the diffusivity of NH_3 and accelerate the reaction rate. It is concluded that the catalytic mechanism of NH_3 absorbing materials on the H_2 generation of the NH_3−LiH system is characteristic and different from the mechanism of conventional metallic catalysts such as Pt on general gas−solid reactions.

Acknowledgements

I am deeply grateful to my supervisor Professor Dr. Yoshitsugu Kojima for his helpful guidance, comments, and suggestions in my doctoral course. I would like to express the deep appreciation to Professor Dr. Takayuki Ichikawa for a lot of valuable guidance and discussion. I would like to show my great appreciation to Associate Professor Dr. Hiroki Miyaoka for helpful advice and thoughtful encouragements. I would like to thank to Professor Dr. Takashi Suzuki and Professor Dr. Takahiro Onimaru for useful suggestions and comments in this work. I am indebted to Dr. Kenichi Kojima in Hiroshima university, Associate Prof. Dr. Hiroshi Tanida in Toyama prefectural university, and Mr. Hitoshi Fujitaka in Hiroshima university for useful discussion and kind help. Finally, I would like to express my sincere thanks to the colleagues of laboratory, Mr. Tomoyuki Ichikawa, Dr. Ankur Jain, Dr. Toru Kimura, Dr. Hitoshi Inokawa, Dr. Liang Zeng, Dr. Sanjay Kumar, Dr. Tengfei Zhang, Dr. Suganthamalar Selvaraj, Ms. Hikaru Miyaoka, Dr. Kiyotaka Goshome, Dr. Koji Kawahito, Dr. Taihei Aoki, Dr. Shotaro Yamaguchi, Mr. Takahiro Okuda, Mr. Chiaying Lu, Mr. Keita Shinzato, Mr. Hironori Kawai, Ms. Pratibha Pal, Ms. Misao Mukoda, and Ms. Saori Inagaki for their kind help and support in my doctoral course.

公表論文

(1) Operando spectroscopic analyses for ammonia absorption process of sodium borohydride
Keita Nakajima, Hiroki Miyaoka, Kenichi Kojima, Takayuki Ichikawa, and Yoshitsugu Kojima
Chemical Communications, in press.

(2) Catalysis of Lithium Chloride and Alkali Metal Borohydrides on Hydrogen Generation of Ammonia and Lithium Hydride System
Hiroki Miyaoka, Keita Nakajima, Shotaro Yamaguchi, Taihei Aoki, Hikaru Yamamoto, Takahiro Okuda, Kiyotaka Goshome, Takayuki Ichikawa, and Yoshitsugu Kojima
The Journal of Physical Chemistry C, **119**, 19922-19927 (2015).

参考論文

(1) Assessment of hydrogen storage property of Ca-Mg-B-H system using NMR and thermal analysis techniques
Sanjay Kumar, Keita Nakajima, Anamika Singh, Yoshitsugu Kojima, and Gautam Kumar Dey
International Journal of Hydrogen Energy, **42**, 26007-26012 (2017).

(2) Improved Hydrogen Release from Magnesium Borohydride by $ZrCl_4$ Additive
Sanjay Kumar, Anamika Singh, Keita Nakajima, Ankur Jain, Hiroki Miyaoka, Takayuki Ichikawa, Gautam Kumar Dey, and Yoshitsugu Kojima
International Journal of Hydrogen Energy, **42**, 22342-22347 (2017).

(3) Synthesis, structural characterization, and hydrogen desorption properties of $Na[Al(NH_2BH_3)_4]$
Yuki Nakagawa, Keita Shinzato, Tessui Nakagawa, Keita Nakajima, Shigehito Isobe, Kiyotaka Goshome, Hiroki Miyaoka, and Takayuki Ichikawa
International Journal of Hydrogen Energy, **42**, 6173-6180 (2017).